

GALAX: GRAPH-AUGMENTED LANGUAGE MODEL FOR EXPLAINABLE REINFORCEMENT-GUIDED SUBGRAPH REASONING IN PRECISION MEDICINE

Heming Zhang¹, Di Huang², Wenyu Li², Michael Province³
 Yixin Chen¹, Philip Payne¹, Fuhai Li^{1*}

¹I2DB, Washington University School of Medicine

²Department of Computer Science and Engineering, Washington University in St. Louis

³Department of Genetics, Washington University School of Medicine

ABSTRACT

In precision medicine, quantitative multi-omic features, topological context, and textual biological knowledge play vital roles in identifying disease-critical signaling pathways and targets, guiding the discovery of novel therapeutics and effective treatment strategies. Existing pipelines capture only one or two of these—numerical omics ignore topological context, text-centric LLMs lack quantitative grounded reasoning, and graph-only models underuse rich node semantics and the generalization power of LLMs—thereby limiting mechanistic interpretability. Although Process Reward Models (PRMs) aim to guide reasoning in LLMs, they remain limited by coarse step definitions, unreliable intermediate evaluation, and vulnerability to reward hacking with added computational cost. These gaps motivate jointly integrating quantitative multi-omic signals, topological structure with node annotations, and literature-scale text via LLMs, using subgraph reasoning as the principle bridge linking numeric evidence, topological knowledge and language context. To resolve this challenge, we propose **GALAX** (Graph Augmented LAnguage model with eXplainability), an innovative framework that integrates pretrained Graph Neural Networks (GNNs) into Large Language Models (LLMs) via reinforcement learning guided by a Graph Process Reward Model (GPRM), which generates disease-relevant subgraphs in a step-wise manner initiated by an LLM and iteratively evaluated by a pretrained GNN, enabling process-level supervision without explicit intermediate reasoning annotations. As an application, we also introduced **Target-QA**, a benchmark combining CRISPR-identified targets, multi-omic profiles, and biomedical graph knowledge across diverse cancer cell lines, which enables GNN pretraining for supervising step-wise graph construction and supports long-context reasoning over text-numeric graphs (TNGs), providing a scalable and biologically grounded framework for explainable, reinforcement-guided subgraph reasoning toward reliable and interpretable target and pathway discovery in precision medicine. The **Target-QA**¹ and **GALAX**² are publicly available at Huggingface and GitHub.

1 INTRODUCTION

Identifying therapeutic targets and elucidating disease mechanisms are main challenges in precision medicine (Steyaert et al., 2023; Topol, 2019). CRISPR-based gene editing has revolutionized functional genomics by enabling high-throughput perturbation of gene function across diverse cellular contexts (Shalem et al., 2014; Li et al., 2023). In oncology, large-scale CRISPR screens in cancer cell lines and patient-derived models have revealed context-specific genetic vulnerabilities, providing a robust experimental foundation for biomarker and target discovery (Shi et al., 2015). Despite these advances, computationally predicting key targets from multi-omic profiles and interpreting their mechanistic role in disease progression remains difficult. In particular, bridging

*Correspondence: Fuhai.Li@wustl.edu

¹Hugging Face: <https://huggingface.co/datasets/FuhaiLiAiLab/Target-QA>

²GitHub: <https://github.com/FuhaiLiAiLab/GALAX>

omic data with interpretable explanations of molecular mechanisms continues to be a critical unmet need (Zhang et al., 2024a). Traditional approaches, such as differential expression analysis or essentiality scoring, lack the capacity to model the hierarchical and cross-modal dependencies in molecular networks, often overlooking key regulatory redundancies and pathway-level dynamics. Recent graph-based models have shown promise in outcome prediction tasks (Ren et al., 2024), yet they typically lack the structured supervision necessary for accurate target prioritization and mechanism discovery and seldom jointly integrate quantitative multi-omic features, topological structure with node annotations, and literature-scale text—limiting mechanistic interpretability.

Meanwhile, Large Language Models (LLMs) have demonstrated strong capabilities in natural language understanding and reasoning, particularly through techniques like in-context learning (ICL) (Brown et al., 2020) and chain-of-thought (CoT) prompting (Wei et al., 2022), which enable multi-step reasoning. However, LLMs often suffer from hallucination and lack grounding in structured knowledge, especially in scientific domains. To mitigate these issues, Retrieval-Augmented Generation (RAG) (Lewis et al., 2020) and its graph-based variants, such as RoG (Luo et al., 2023) and G-Retriever (He et al., 2024), have been proposed to enhance LLM performance by incorporating external knowledge graph. Despite their utility, these methods primarily optimize for outcome-level accuracy, often neglecting the interpretability and reliability of intermediate reasoning steps. Moreover, they operate over purely textual graphs, limiting their ability to incorporate high-dimensional, personalized numerical data, such as multi-omic profiles, especially when the input context becomes large and complex, and to respect biological topology at scale when the input context becomes large and complex. On the other hand, the Process Reward Model (PRM) framework has been introduced to provide fine-grained supervision over intermediate steps in reasoning tasks (Luo et al.; Lightman et al., 2023; Uesato et al., 2022; Wang et al., 2023). PRMs provide step-wise supervision by assigning intermediate rewards to reinforcement learning (RL) agents, forming the foundation for Large Reasoning Models (LRMs) trained with Reinforcement Learning with Human Feedback (RLHF) (Bai et al., 2022), Proximal Policy Optimization (PPO) (Schulman et al., 2017), and Group Relative Policy Optimization (GRPO) (Shao et al., 2024). For example, StepGRPO (Zhang et al., 2025b) extends GRPO by incorporating rule-based step-wise rewards to supervise each intermediate reasoning step, addressing the sparse reward problem and enhancing multi-step reasoning in multimodal language models. However, PRMs face key limitations in defining fine-grained reasoning steps, verifying intermediate correctness, and hacking for model-based rewards (Gao et al., 2023), further complicating training.

These challenges are amplified in biomedicine: reasoning over multi-omic, gene-regulatory text–numeric graphs (TNGs) lacks ground-truth stepwise annotations, making intermediate supervision infeasible, and the combinatorial explosion of biological paths renders exhaustive planning or retrieval impractical. We propose **GALAX** (**G**raph-**A**ugmented **L**anguage model with **e**Xplainability), which couples LLMs with a pretrained GNN under reinforcement learning guided by a **Graph Process Reward Model (GPRM)**. Instead of symbolic traces or manual labels, GALAX uses the GNN as a proxy stepwise supervisor, scoring intermediate subgraphs (partial signaling cascades) for biological plausibility and cancer relevance to provide fine-grained, graph-based rewards. GALAX prompts an LLM to propose candidate targets from multi-omic profiles and partial knowledge graphs, then an RL graph generator assembles task-specific cancer subnetworks under GPRM scoring—translating language reasoning into interpretable graph construction and yielding mechanistically grounded, patient-specific subnetworks for target prioritization. To evaluate, we introduce **Target-QA**, a benchmark integrating multi-omic data, biomedical graph knowledge, and CRISPR screening outcomes across diverse cancer cell lines. Together, GALAX and Target-QA deliver a scalable, reinforcement-guided solution for interpretable, patient-specific target identification and disease-mechanism discovery.

2 RELATED WORK

LLMs Augmented with Knowledge and Graph Structures Prompt tuning has emerged as a lightweight and scalable method for adapting LLMs to downstream tasks without full fine-tuning (Korbak et al., 2023; Lester et al., 2021). While effective, it operates over flat text representations and struggles to incorporate structured domain knowledge or multi-modal signals. To address this, Retrieval-Augmented Generation (RAG) (Lewis et al., 2020), Chain-of-Thought (CoT) prompting (Wei et al., 2022), and graph-augmented approaches such as GraphRAG and G-Retriever (He et al., 2024) have been proposed to provide external knowledge and user-conditioned

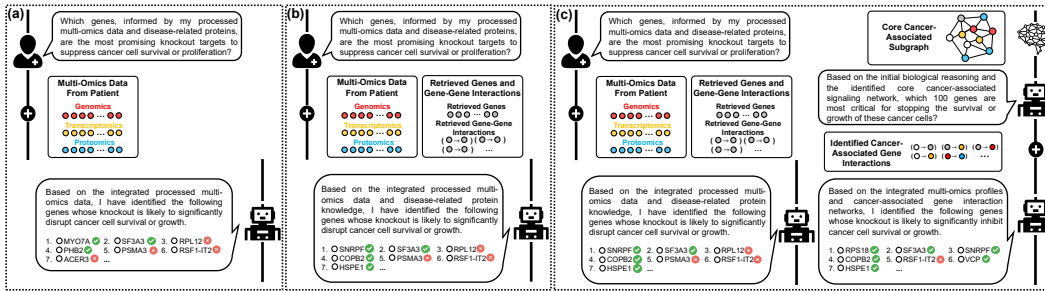


Figure 1: Representative paradigms of patient-specific target prediction in-context LLM workflows and comparison with our approach. (a) User-specific in-context prompts with basic query input. **(b)** Augmentation with retrieved knowledge relevant to the query. **(c)** GALAX framework: combining user-specific prompts, biomedical knowledge, and reinforcement-guided subgraph reasoning for explainable target prediction.

reasoning. RoG (Luo et al., 2023) further embeds relational graph information into prompts to improve performance. However, these methods rely on unsupervised graph construction and do not support reliable reasoning. Furthermore, their reliance on purely textual inputs and limited context windows makes them ill-suited for integrating large-scale, patient-specific text-numeric graphs such as multi-omic signaling networks.

Reinforcement Learning for Step-wise Reasoning Reinforcement learning has been instrumental in aligning LLM behavior through methods like RLHF (Bai et al., 2022), PPO (Schulman et al., 2017), and GRPO. The Process Reward Model (PRM) (Luo et al.) enables step-wise supervision and has been adopted in Large Reasoning Models (LRMs). However, PRMs face key challenges: fine-grained step definitions are ambiguous, intermediate correctness is hard to validate, and model-based rewards can lead to reward hacking (Gao et al., 2023). These challenges are particularly acute in biomedical domains, where reasoning is inherently unstructured and lacks step-wise annotations, making conventional PRM pipelines impractical.

Multi-omic Data Integration in Biomedical AI From a biological standpoint, the integration of genomic, transcriptomic, and proteomic has been essential for understanding disease mechanisms and therapeutic vulnerabilities (Hasin et al., 2017; Kristensen et al., 2014). Traditional approaches rely on statistical fusion or dimensionality reduction (Meng et al., 2016; Shen et al., 2009; Rohart et al., 2017; Argelaguet et al., 2018; Nguyen & Wang, 2020), which overlook the hierarchical and interconnected nature of molecular data. More recently, GNN-based models like MOGONET (Wang et al., 2021) and MoGCN (Li et al., 2022) have demonstrated the value of structured graph reasoning for cancer subtype classification and biomarker identification. However, these models are primarily designed for outcome prediction and often fall short in identifying actionable biomarkers associated with specific disease mechanisms.

GALAX addresses the limitations of existing models by introducing a RL-guided framework that dynamically constructs biologically relevant subgraphs for each patient or cell line. This enables interpretable, context-sensitive target prioritization that adapts to both multi-omic features and disease-specific graph as the text-numeric format. To our knowledge, GALAX is the first to unify multi-omic integration, graph-augmented reasoning, and LLMs under a reinforcement learning paradigm with biologically grounded supervision, which learns to reason through step-wise subgraph generation, guided by an authoritative biomedical GRPM.

3 PROBLEM FORMULATION

Identifying key targets and uncovering disease mechanisms remains a major challenge in precision medicine. To address this, we adopt the Text-Omic Signaling Graph (TOSG) (Zhang et al., 2025a), which integrates multi-omic features and biomedical context into a unified graph structure. Built upon TOSG, our model **GALAX** couples LLM-based hypothesis generation with reinforcement-guided subgraph reasoning to enable interpretable, patient-specific target predictions on the Target-QA benchmark.

TOSG Construction Given the multi-omic dataset of $\mathcal{X}^{(0)} = \{X_1^{(0)}, X_2^{(0)} \dots, X_{n^{(0)}}^{(0)}, \dots, X_{N^{(0)}}^{(0)}\}$, where $X_n^{(0)} \in \mathbb{R}^M$ is composed of multiple components derived from genomic, transcriptomic and proteomic context. Together with those samples collected from DepMap (Dempster et al.), it is attached with binary label for cancerous or non-cancerous cell line with $\mathcal{Y}^{(0)} = \{y_1^{(0)}, y_2^{(0)} \dots, y_{n^{(0)}}^{(0)}, \dots, y_{N^{(0)}}^{(0)}\}$. These multi-omic features being integrated into TOSG by existed integration tool, BioMedGraphica (Zhang et al., 2024b), resulting with text-attributed knowledge graph $\mathcal{G} = \{\mathcal{V}, \mathcal{E}\}$, $\mathcal{V} = \{\mathcal{V}^{(pm)}, \mathcal{V}^{(g)}, \mathcal{V}^{(t)}, \mathcal{V}^{(p)}\}$ represents the set of vertices, where $|\mathcal{V}^{(pm)}| = m^{(pm)}$, $|\mathcal{V}^{(g)}| = m^{(g)}$, $|\mathcal{V}^{(t)}| = m^{(t)}$, $|\mathcal{V}^{(p)}| = m^{(p)}$ and $|\mathcal{V}| = m^{(pm)} + m^{(g)} + m^{(t)} + m^{(p)} = M$. Correspondingly, entities or nodes in TOSG will be mapped with cell-specific omic feature with $X_n^{(0)} = \{pm_1^{(n)}, pm_2^{(n)}, \dots, pm_{m^{(pm)}}^{(n)}, g_1^{(n)}, g_2^{(n)}, \dots, g_{m^{(g)}}^{(n)}, t_1^{(n)}, t_2^{(n)}, \dots, t_{m^{(t)}}^{(n)}, p_1^{(n)}, p_2^{(n)}, \dots, p_{m^{(p)}}^{(n)}\}$, where $pm, g, t,$ and p denote promoter, gene, transcript, and protein-level features, respectively. Meanwhile, each entities or nodes in TOSG has the name and description about it with $\mathcal{T} = \{T_{name}, T_{desc}\}$, where $|T_{name}| = |T_{desc}| = M$. In details, this graph can be decomposed into two subgraphs: $\mathcal{G}^{(in)} = (\mathcal{V}^{(in)}, \mathcal{E}^{(in)})$ and $\mathcal{G}^{(PPI)} = (\mathcal{V}^{(PPI)}, \mathcal{E}^{(PPI)})$. Here, $\mathcal{G}^{(in)}$ captures the internal signaling processes for protein translation (as shown in Figure 2, internal propagation follows the central dogma (Crick, 1970) (promoter (purple)→gene (red)→transcript (yellow)→protein (blue)), with $\mathcal{V} = \mathcal{V}^{(in)}$ and $|\mathcal{V}^{(in)}| = M$, while $\mathcal{G}^{(PPI)}$ represents the gene regulatory network, structured around protein-protein interactions (PPI), where $\mathcal{V}^{(PPI)} = \mathcal{V}^{(p)}$.

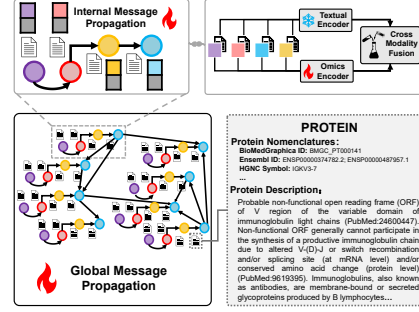


Figure 2: Demonstration of TOSG Construction and Graph Foundation Model

Target-QA Generation We construct Target-QA using cancer cell lines with available CRISPR-based target information, each represented by multi-omic vector $X_n \in \mathbb{R}^M$, forming the set $\mathcal{X} = \{X_1, X_2, \dots, X_n, \dots, X_N\}$. Due to input token constraints of LLMs (Achiam et al., 2023) and the presence of CpG sites with methylation beta values saturated at 1, which dominate rankings and render top- K selection uninformative, we selected the top K features only from genomic, transcriptomic, and proteomic modalities to construct a concise multi-omic representation: $X_n^{(K)} = \{g_1^{(n)}, g_2^{(n)}, \dots, g_K^{(n)}, t_1^{(n)}, t_2^{(n)}, \dots, t_K^{(n)}, p_1^{(n)}, p_2^{(n)}, \dots, p_K^{(n)}\}$, corresponding to omic-related graph nodes $\mathcal{V}_n^{(omic)}$. Each cell line is additionally annotated with disease information curated from BioMedGraphica’s disease-target interaction graph $\mathcal{G}^{(DTI)} = \{\mathcal{V}^{(DTI)}, \mathcal{E}^{(DTI)}\}$, where $\mathcal{V}^{(DTI)} = \{\mathcal{V}^{(S)}, \mathcal{V}^{(p)}\}$ includes disease and protein nodes. And disease entity has an associated name and textual description with $\mathcal{S} = \{S_{name}, S_{desc}\}$ where $|\mathcal{S}| = M^{(S)}$. Cell lines and their disease labels form the sets $\mathcal{C} = \{c_1, c_2, \dots, c_n, \dots, c_N\}$ and $\mathcal{S}' = \{s'_1, s'_2, \dots, s'_n, \dots, s'_N\}$, respectively, based on annotations from DepMap (Dempster et al.). To provide structured graph context, we apply a subgraph retrieval strategy that extracts disease-relevant protein entities $\mathcal{V}_n^{(p)} \subset \mathcal{V}^{(p)}$ and their interactions $\mathcal{E}^{(DTI)}$, along with h -hop protein neighbors $\mathcal{V}_n^{(h)}$ by extracting interactions from $\mathcal{E}^{(PPI)}$, where $\mathcal{V}_n^{(h)} \subset \mathcal{V}^{(p)}$. This yields a sample-specific subgraph $\mathcal{G}_n^{(sub)} = \{\mathcal{V}_n^{(sub)}, \mathcal{E}_n^{(sub)}\}$, where $\mathcal{V}_n^{(sub)} = \mathcal{V}_n^{(p)} \cup \mathcal{V}_n^{(h)}$, with the full graph set $\mathcal{G}^{(sub)} = \{\mathcal{G}_1^{(sub)}, \mathcal{G}_2^{(sub)} \dots, \mathcal{G}_n^{(sub)}, \dots, \mathcal{G}_N^{(sub)}\}$. Hence, each query $Q_n = \{c_n, s'_n, X_n^{(K)}, \mathcal{G}_n^{(sub)}\}$ is paired with answer A_n describing top- γ CRISPR targets $R_n = \{r_{n,1}, \dots, r_{n,\gamma}\}$, yielding instance $D_n = (Q_n, A_n)$ in dataset $\mathcal{D} = \{D_1, \dots, D_N\}$, stratified by TCGA (Weinstein et al., 2013) types (e.g., $\mathcal{D}_{LUAD}, \mathcal{D}_{BRCA}$).

Patient-Specific Target Prediction with Explainability GALAX is designed to generate not only accurate but also interpretable predictions by explicitly modeling the reasoning process through subgraph construction (see Figure 3). Given a query Q_n , the model produces both a prioritized target list \hat{A}_n and an explanatory subgraph \mathcal{G}_n^\dagger :

$$\hat{A}_n, \mathcal{G}_n^\dagger = f(Q_n, X_n, \mathcal{T}, \mathcal{E}; \theta_G, \theta_L) \quad (1)$$

The function f is composed of three modules (see Section 4.2): (1) an initial language model f_{init} that performs coarse reasoning and extracts candidate entities via initial answering; (2) a reinforcement-based graph generator $\pi(\cdot)$ that incrementally constructs the explainable subgraph \mathcal{G}_n^\dagger under the

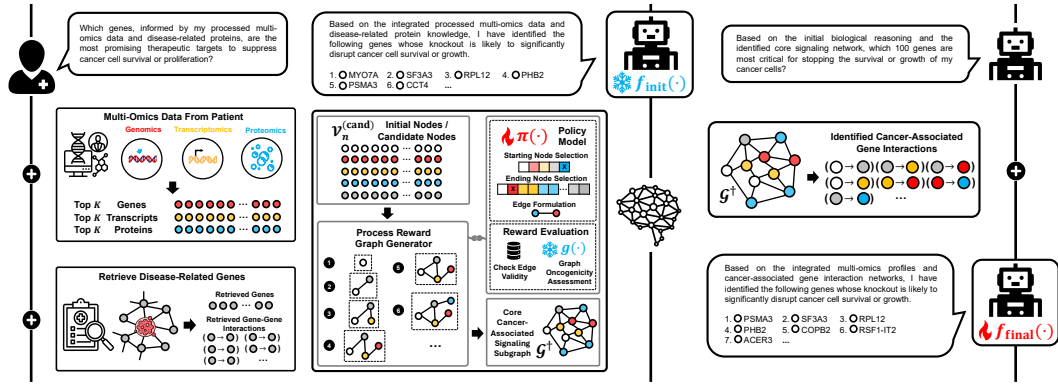


Figure 3: An overview of the GALAX workflow. Given processed multi-omic profiles (genomic, transcriptomic, proteomic), a subgraph is retrieved by identifying disease-associated proteins and their h -hop neighbors. Then $f_{\text{init}}(\cdot)$ proposes initial targets, refined by a reinforcement-guided graph generator $\pi(\cdot)$ supervised by a pretrained graph foundation model $g(\cdot)$. The final subgraph, \mathcal{G}^\dagger , combined with the query, is passed to a second-stage LLM $f_{\text{final}}(\cdot)$ for target prediction. The full pipeline enables explainable, patient-specific reasoning grounded in molecular biology and CRISPR evidence.

guidance of a pretrained graph classifier $g(\cdot)$ parameterized by θ_G , using step-wise biological plausibility rewards; and (3) a final language model f_{final} that refines the prediction by reasoning over both the initial output and the generated subgraph context. The subgraph \mathcal{G}_n^\dagger serves as a transparent rationale, offering deeper insights into the disease mechanism.

4 GALAX

4.1 FOUNDATION MODELS PRETRAINING

LLM Pretraining We pretrain a large language model, denoted as f_L^{pre} with parameters θ_L^{pre} , using curated text corpora. The input data comprises omic entity descriptions \mathcal{T} , disease annotations \mathcal{S} , protein–protein interactions $\mathcal{E}^{(\text{PPI})}$, and drug–target relationships $\mathcal{E}^{(\text{DTI})}$. As illustrated in Figure 5, this pretraining phase equips the model with foundational knowledge of biomedical terminology and relational structure (see Appendix C.1), thereby enhancing its capacity for downstream reasoning in biomedical tasks. Then we will continue pretraining the language model f_{init} parameterized by θ_{init} , which are detailed in Appendix C.2.

Graph Foundation Model Pretraining We pretrain the graph encoder θ_G^{pre} via a two-stage pipeline (see Figure 2). In stage one, a unified graph–language model f_G^{pre} is trained over node attributes $\mathcal{X}^{(0)}$, textual features \mathcal{T} , and edge set \mathcal{E} , with protein–protein interaction edges stochastically masked as $\mathcal{E}_{\text{mask}} \sim \text{Bernoulli}(p)$, $p < 1$. The resulting representation is

$$\mathcal{H}^{\text{pre}} = f_G^{\text{pre}}(\mathcal{X}^{(0)}, \mathcal{T}, \mathcal{E}, \mathcal{E}_{\text{mask}}) \quad (2)$$

, where $\mathcal{H}^{\text{pre}} \in \mathbb{R}^{N^{(0)} \times M \times d^{(\text{pre})}}$ encodes contextualized entity states. In details, we generate edge mask $\mathcal{E}_{\text{mask}} \sim \text{Bernoulli}(p)$, where $p < 1$ is the ratio of the masked edges for $\mathcal{E}^{(\text{PPI})}$ to mask out the signaling flows in protein-protein interactions. Then, we apply internal message propagation with

$$\mathcal{H}_{\text{in}}^{\text{pre}} = \text{GNN}_{\text{in}}^{\text{pre}}(\text{ENC}_{\text{cross}}^{\text{pre}}(\mathcal{X}^{(0)}, \mathcal{T}), \mathcal{E}^{(\text{in})}) \quad (3)$$

, where $\text{ENC}_{\text{cross}}^{\text{pre}}$ is a cross-modal encoder to align textual and omic features and $\mathcal{H}_{\text{in}}^{\text{pre}} \in \mathbb{R}^{N^{(0)} \times M \times d^{(\text{in})}}$. The first-stage pretraining captures gene regulatory patterns by performing masked global message passing over $\mathcal{E}^{(\text{PPI})}$ by

$$\mathcal{H}^{\text{pre}} = \text{GNN}_{\text{PPI}}^{\text{pre}}(\mathcal{H}_{\text{in}}^{\text{pre}}, \mathcal{E}^{(\text{PPI})}, \mathcal{E}_{\text{mask}}) \quad (4)$$

In the second stage, downstream model f_G is initialized with pretrained parameters θ_G^{pre} and is used to predict disease types from multi-omic inputs. The predicted class for each sample is given by:

$$\hat{\mathcal{Y}}^{(0)} = \arg \max_{o \in \mathcal{O}} \text{Softmax} \left[\text{MLP}_G \left(f_G(\mathcal{X}^{(0)}, \mathcal{T}, \mathcal{E}; \theta_G^{\text{pre}}) \right) \right] \quad (5)$$

, where \mathcal{O} denotes the set of disease types, and f_G consists of the same architecture as $\text{ENC}_{\text{cross}}$, GNN_{in} , and GNN_{ppi} . The model is trained to minimize the cross-entropy loss between the predicted probability distribution by $\text{Softmax}[\text{MLP}_G(f_G(\cdot))]$ and the ground-truth label. The pretrained graph foundation model f_G serves as a structural proxy to guide step-wise reasoning in downstream tasks.

4.2 MODEL TRAINING

The pipeline of model couples initial answering, a reinforcement-guided subgraph generator, and final answering. Given the structured prompt $P_n^{(\text{init})}$ from query Q_n , the pretrained model f_{init} outputs $A_n^{(\text{init})}$ and a biomedical named entity recognition (NER) ϕ extracts entities $R_n^{(\text{init})}$ and maps them to proteins $\mathcal{V}_n^{(\text{init})}$, which will contribute to forming the start set $\mathcal{V}_n^{(\text{start})}$ depending on situation. Node features are embedded by pretrained graph foundation model to obtain \mathcal{H}_{in} and formed $X_n^{(\text{cand})}$. Sub-graph construction is framed as reinforcement learning problem consisting of four elements: **state** $\mathcal{G}_n^{(i)} = (\mathcal{V}_n^{(i)}, \mathcal{E}_n^{(i)})$; **action** $\Delta_n^{(i)} = (v_{\text{src}}^i, v_{\text{tgt}}^i)$ adds a single edge under feasibility masks; **policy** uses a message propagation (MSG) module to produce $X_n^{(i)} = \pi_{\text{MSG}}(\mathcal{G}_n^{(i)}, X_n^{(\text{cand})})$ and two masked probability function $\pi_{\text{SRC}}, \pi_{\text{TGT}}$ to sample v_{src}^i and v_{tgt}^i ; **reward** combines feedback from a pretrained classifier $g(\cdot)$, a rollout averaging L simulated continuations, and a rule-based term $\mathcal{R}_{\text{rule}}$ that penalizes schema violations. We accept an action e only when $\mathcal{R}_{\text{total}}^{(i)} > 0$ and update the generator with reward-weighted cross-entropy with early stopping; the best subgraph \mathcal{G}_n^\dagger is retained in Ω stochastic run. For final answering, \mathcal{G}_n^\dagger is verbalized in expert mode (Fatemi et al., 2023) and appended to Q_n to form $P_n^{(\text{final})}$; the model f_{final} is finetuned with token-level cross-entropy against A_n . What follows is a detailed exposition of the model design and training framework.

Initial Answering With the pretrained language model f_{init} based on f_L , parameterized by θ_{init} , the input to the model is a structured prompt $P_n^{(\text{init})}$ derived from the original query Q_n , specifically for turning $\mathcal{G}_n^{(\text{sub})}$ into a graph expert format (see Appendix C.2 for details), and it will output $A_n^{(\text{init})}$. Afterwards, an NER function, ϕ , is applied to extract biomedical entities from $A_n^{(\text{init})}$ by $R_n^{(\text{init})} = \phi(A_n^{(\text{init})})$, where $R_n^{(\text{init})} = \{r_{n,1}^{(\text{init})}, r_{n,2}^{(\text{init})}, \dots, r_{n,\alpha}^{(\text{init})}\}$. And which are then mapped to corresponding protein nodes, $\mathcal{V}_n^{(\text{init})} = \{v_{n,\text{init},1}^{(p)}, v_{n,\text{init},2}^{(p)}, \dots, v_{n,\text{init},\alpha'}^{(p)}\}$.

Process Reward Graph Generator The initial node set $\mathcal{V}_n^{(\text{start})}$ is selected based on a predefined priority: if the disease-related protein set $\mathcal{V}_n^{(p)}$ is available, the top η most relevant entities are used; if not, the top η entities from the initialization set $\mathcal{V}_n^{(\text{init})}$ are selected. If both are unavailable, η nodes are randomly sampled from the omic-derived set $\mathcal{V}_n^{(\text{omic})}$. Formally,

$$\mathcal{V}_n^{(\text{start})} = \begin{cases} \text{Top-}\eta(\mathcal{V}_n^{(p)}), & \text{if } \mathcal{V}_n^{(p)} \neq \emptyset \\ \text{Top-}\eta(\mathcal{V}_n^{(\text{init})}), & \text{else if } \mathcal{V}_n^{(\text{init})} \neq \emptyset \\ \text{Sample-}\eta(\mathcal{V}_n^{(\text{omic})}), & \text{otherwise} \end{cases} \quad (6)$$

The candidate set was generated based on $\mathcal{V}_n^{(\text{cand})} = \mathcal{V}_n^{(\text{init})} \cup \mathcal{V}_n^{(\text{sub})} \cup \mathcal{V}_n^{(\text{omic})}$ and $\mathcal{V}_n^{(\text{start})} \subset \mathcal{V}_n^{(\text{cand})}$. And the features of \mathcal{X} are precomputed using a graph encoder f_G^{pre} with parameters θ_G^{pre} , followed by pretrained modules $\text{ENC}_{\text{cross}}$ and GNN_{in} with parameters θ_{cross}^G and θ_{in}^G , respectively:

$$\mathcal{H}_{\text{in}} = \text{GNN}_{\text{in}} \left(\text{ENC}_{\text{cross}} \left(f_G^{\text{pre}}(\mathcal{X}, \mathcal{T}, \mathcal{E}; \theta_G^{\text{pre}}), \mathcal{T}; \theta_{\text{cross}}^G \right), \mathcal{E}^{(\text{in})}; \theta_{\text{in}}^G \right) \in \mathbb{R}^{N \times M \times d^{(\text{in})}} \quad (7)$$

The candidate node features $X_n^{(\text{cand})}$ are selected from the precomputed representation \mathcal{H}_{in} . Then we introduce a reinforcement-guided graph generator, denoted as $\pi(\cdot)$, where the policy operates over sample-specific graph states and candidate sets, enabling personalized subgraph construction. At step i , the current graph state is defined as $\mathcal{G}_n^{(i)} = \{\mathcal{V}_n^{(i)}, \mathcal{E}_n^{(i)}\}$ after applying the action of constructing edge $(v_{\text{src}}^i, v_{\text{tgt}}^i)$. The next graph state $\mathcal{G}_n^{(i+1)}$ is formed by adding an edge between a sampled source node v_{src}^i and target node v_{tgt}^i . To compute the probabilities of selecting these nodes, we embed the node features from $\mathcal{G}_n^{(i)}$ together with the candidate features $X_n^{(\text{cand})}$ as:

$$X_n^{(i)} = \pi_{\text{MSG}}(\mathcal{G}_n^{(i)}, X_n^{(\text{cand})}) \quad (8)$$

, where π_{MSG} consists of a message propagation (MSG) module and a feature selection mechanism that extracts node embeddings corresponding to $\mathcal{V}_n^{(i)}$ from the propagated features. Based on embeddings, the source and target nodes are sampled according to the generated probabilities with

$$v_{\text{src}}^i \sim \pi_{\text{SRC}}(X_n^{(i)}, \mathcal{M}_{\text{SRC}}); \quad v_{\text{tgt}}^i \sim \pi_{\text{TGT}}(X_n^{(i)}, \mathcal{M}_{\text{TGT}}; v_{\text{src}}^i) \quad (9)$$

, where π_{SRC} and π_{TGT} are returned with probability implemented via MLPs and softmax by masking \mathcal{M}_{SRC} and \mathcal{M}_{TGT} , which restrict source selection to nodes in $\mathcal{G}_n^{(i)}$ and exclude the source when selecting the target. Based on the probability, nodes v_{src}^i and v_{tgt}^i will be selected by the sampling function. The selected node pair then forms the updated graph state $\mathcal{G}_n^{(i+1)}$ for next step.

Reinforcement-Guided Reward and Training To guide the graph generation process, we define a rollout-based reward function that combines immediate classifier feedback with future trajectory simulation. At generation step i , the intermediate graph is represented as $\mathcal{G}_n^{(i+1)} = \{\mathcal{V}_n^{(i+1)}, \mathcal{E}_n^{(i+1)}\}$ after applying the action of constructing edge $(v_{\text{src}}^i, v_{\text{tgt}}^i)$. We define $g(\cdot)$ as a pretrained graph classifier that computes class probabilities by applying a GNN encoder $\text{GNN}_{\text{PPI}}^{\text{G}}$ followed by a projection head MLP_{G} , formally expressed as $g(\cdot) = \text{Softmax}[\text{MLP}_{\text{G}}(\text{GNN}_{\text{PPI}}^{\text{G}}(\cdot))]$. The model is parameterized by pretrained weights $\theta_{\text{PPI}}^{\text{G}}$ and $\theta_{\text{MLP}}^{\text{G}}$, and outputs a probability distribution over classes in \mathcal{O} . Let $o^* \in \mathcal{O}$ denote the target class. The reward $\mathcal{R}_n^{(i)}$ for step i is defined as:

$$\mathcal{R}_n^{(i)} = g_{o^*}(\mathcal{G}_n^{(i+1)}) - \frac{1}{|\mathcal{O}|} + \lambda \cdot \frac{1}{L} \sum_{\ell=1}^L \left[g_{o^*}(\text{Rollout}_{\ell}(\mathcal{G}_n^{(i+1)})) - \frac{1}{|\mathcal{O}|} \right] \quad (10)$$

Here, $g_{o^*}(\mathcal{G})$ refers to the probability assigned to the target class o^* , and $\text{Rollout}_{\ell}(\cdot)$ simulates the ℓ -th full trajectory by continuing generation from the current partial graph using the current policy. The hyperparameter λ balances intermediate and future rollout-based feedback. To ensure reasoning aligning with biological plausibility, we incorporate a rule-based reward term $\mathcal{R}_{\text{rule}}(\mathcal{G}_n^{(i+1)})$ that penalizes invalid edges according to relations from BioMedGraphica. The final reward is:

$$\mathcal{R}_{\text{total}}^{(i)} = \mathcal{R}_n^{(i)} + \lambda_{\text{rule}} \cdot \mathcal{R}_{\text{rule}}(\mathcal{G}_n^{(i+1)}) \quad (11)$$

This formulation guides the generation process toward subgraphs that are both predictive of the target class and consistent with domain-specific biological priors. And we used the greedy acceptance where if $\mathcal{R}_{\text{total}}^{(i)} > 0$, set $\mathcal{G}_n^{(i+1)}$ as current state; otherwise keep the previous state. Then in each step i , the model will be trained with loss function,

$$\mathcal{L}_{\text{step}} = -\mathcal{R}_{\text{total}}^{(i)} [\text{CE}(v_{\text{src}}^i, \pi_{\text{SRC}}(X_n^{(i)}, \mathcal{M}_{\text{SRC}})) + \text{CE}(v_{\text{tgt}}^i, \pi_{\text{TGT}}(X_n^{(i)}, \mathcal{M}_{\text{TGT}}; v_{\text{src}}^i))] \quad (12)$$

, where the generator is optimized with reward-weighted cross-entropy (CE) function. In practice, we sample multiple candidate subgraphs under the policy parameterized by θ_{π} across multiple runs Ω , and select the optimal subgraph \mathcal{G}_n^{\dagger} .

Final Answer Generation with Prompt Tuning The optimal subgraph \mathcal{G}_n^{\dagger} is converted into a structured textual description via expert mode (see details in Appendix D.1), which will be appended to original query Q_n to form final graph-augmented prompt $P_n^{(\text{final})}$. With language model f_{final} based on pretrained f_{init} , it generates the output sequence $\hat{A}_n = \{\hat{a}_{n,1}, \hat{a}_{n,2}, \dots, \hat{a}_{n,J'}\}$ according to:

$$\xi_{\theta_{\text{final}}}(\hat{A}_n | Q_n, \mathcal{G}_n^{\dagger}) = \prod_{j=1}^{J'} \xi_{\theta_{\text{final}}}(\hat{a}_{n,j} | \hat{a}_{n,<j}, P_n^{(\text{final})}) \quad (13)$$

To align the model output with the refined ground-truth answer A_n , which contains the top γ CRISPR-prioritized gene targets for sample n , we finetune the model by:

$$\mathcal{L}_{\text{final}} = -\sum_{n=1}^N \sum_{j=1}^{J'} \log \xi_{\theta_{\text{final}}}(a_{n,j} | a_{n,<j}, P_n^{(\text{final})}) \quad (14)$$

This objective encourages the model to internalize the structured reasoning encoded in \mathcal{G}_n^{\dagger} to generate biologically grounded answers. After generation, an NER function ϕ will extract entities from the model’s output \hat{A}_n with $\hat{R}_n = \phi(\hat{A}_n) = \{\hat{r}_{n,1}, \hat{r}_{n,2}, \dots, \hat{r}_{n,\beta}\}$. These predicted protein targets are used for evaluating biological relevance and overlap within reference targets in A_n .

5 EXPERIMENTS

Datasets We construct the Target-QA dataset over multiple TCGA cancer types using DepMap, integrating multi-omic features (epigenomic, genomic, transcriptomic, proteomic) and metadata from cancer cell lines. Each QA pair consists of an input query, including multi-omic and cell line information, and an output answer comprising the top- γ ($\gamma = 100$) CRISPR-prioritized targets. The final dataset contains 363 QA pairs from cancerous cell lines after integration and preprocessing. We use an 80/20 train-test split and repeat experiments across four randomized seeds to ensure stability and generalization. For foundation model pretraining, we collect dataset of 336 samples with multi-omic features from unannotated samples, including both disease and control groups (297 cancerous, 39 non-cancerous), and apply stratified sampling to address class imbalance. Full data processing and cohort composition are described in Appendix B).

Experimental Setup We initialize the language model with LLaMA3-8B-Instruct (AI@Meta, 2024), pretrained on biomedical terminology and curated textual descriptions involving protein-protein and disease-protein relationships from BioMedGraphica to enhance domain-specific vocabulary and biological context understanding (see Figure 5). For graph encoding, we use BioBERT-v1.1 (Lee et al., 2020) for text embeddings and Graph Attention Networks (GAT) (Veličković et al., 2017) to learn topological features from protein interaction graphs, incorporating random edge masking to improve robustness (see Figure 2 global message propagation). The pretrained GNN achieves 64.4% AUC in edge prediction, and 99.46% / 96.15% accuracy on disease type classification (train/test). Named entities are extracted using GPT-4o-mini via ChatGPT API (OpenAI, 2023). GALAX is trained using the Adam optimizer on two NVIDIA H100 GPUs (80GB). We set the number of top omic features per modality to $K=10$, the maximum subgraph rollout depth to $L=5$, and the number of candidate starting nodes $\eta=20$. The reward formulation includes both rollout- and rule-based components, each weighted equally with $\lambda=1$ and $\lambda_{\text{rule}}=1$. The reasoning task is formulated as a binary classification problem ($|\mathcal{O}|=2$), using a 1-hop ($h=1$) protein neighborhood from the disease-annotated subgraph. Model outputs are evaluated using precision, recall, F1-score, Jaccard similarity, Hit@5 and Hit@10, by comparing predicted target sets \hat{R}_n against reference labels R_n . Additional details are provided in the Appendix D.2.

Table 1: Performance of models across datasets and metrics

Model	Overall		LUAD		BRCA	
	Precision \uparrow	Recall \uparrow	Precision \uparrow	Recall \uparrow	Precision \uparrow	Recall \uparrow
M2T	0.0016	0.0011	0.0020	0.0014	0.0000	0.0000
GAT	0.0006 \pm 0.0000	0.0006 \pm 0.0000	0.0000 \pm 0.0000	0.0000 \pm 0.0000	0.0033 \pm 0.0000	0.0033 \pm 0.0000
L3 + Omics	0.0071 \pm 0.0032	0.0013 \pm 0.0002	0.0079 \pm 0.0137	0.0005 \pm 0.0008	0.0020 \pm 0.0035	0.0017 \pm 0.0029
L3 + Omics + KG	0.0125 \pm 0.0032	0.0029 \pm 0.0003	0.0014 \pm 0.0025	0.0010 \pm 0.0017	0.0073 \pm 0.0068	0.0033 \pm 0.0029
L3-FT(Med) + Omics	0.0179 \pm 0.0045	0.0133 \pm 0.0064	0.0091 \pm 0.0018	0.0105 \pm 0.0044	0.0110 \pm 0.0086	0.0106 \pm 0.0075
L3-FT(Med) + Omics + KG	0.0158 \pm 0.0030	0.0058 \pm 0.0011	0.0081 \pm 0.0071	0.0024 \pm 0.0017	0.0149 \pm 0.0057	0.0050 \pm 0.0000
L3-FT(QA) + Omics	0.5250 \pm 0.0282	0.4959 \pm 0.0435	0.5201 \pm 0.0408	0.4905 \pm 0.0532	0.5074 \pm 0.0498	0.4856 \pm 0.0570
L3-FT(QA) + Omics + KG	0.5185 \pm 0.0240	0.4908 \pm 0.0402	0.5214 \pm 0.0242	0.4952 \pm 0.0432	0.4856 \pm 0.0395	0.4656 \pm 0.0436
G-Retriever + pre-GAT	0.4763 \pm 0.0004	0.3929 \pm 0.0063	0.4642 \pm 0.0181	0.3881 \pm 0.0264	0.4414 \pm 0.0099	0.3772 \pm 0.0010
GALAX	0.5472\pm0.0053	0.5332\pm0.0031	0.5345\pm0.0185	0.5157\pm0.0043	0.5608\pm0.0031	0.5533\pm0.0033

Table 2: Hit@10 and Hit@5 for models across datasets

Model	Overall		LUAD		BRCA	
	Hit@10 \uparrow	Hit@5 \uparrow	Hit@10 \uparrow	Hit@5 \uparrow	Hit@10 \uparrow	Hit@5 \uparrow
M2T	0.0029	0.0000	0.0000	0.0000	0.0000	0.0000
GAT	0.0000 \pm 0.0000					
L3 + Omics	0.0021 \pm 0.0037	0.0032 \pm 0.0055	0.0048 \pm 0.0082	0.0095 \pm 0.0165	0.0000 \pm 0.0000	0.0000 \pm 0.0000
L3 + Omics + KG	0.0122 \pm 0.0033	0.0085 \pm 0.0037	0.0000 \pm 0.0000	0.0000 \pm 0.0000	0.0056 \pm 0.0096	0.0111 \pm 0.0192
L3-FT(Med) + Omics	0.0122 \pm 0.0072	0.0116 \pm 0.0097	0.0000 \pm 0.0000	0.0000 \pm 0.0000	0.0111 \pm 0.0192	0.0000 \pm 0.0000
L3-FT(Med) + Omics + KG	0.0132 \pm 0.0040	0.0106 \pm 0.0048	0.0048 \pm 0.0082	0.0095 \pm 0.0165	0.0111 \pm 0.0192	0.0000 \pm 0.0000
L3-FT(QA) + Omics	0.8693 \pm 0.0157	0.8889 \pm 0.0168	0.8667 \pm 0.0218	0.8476 \pm 0.0165	0.8389 \pm 0.0096	0.8889 \pm 0.0509
L3-FT(QA) + Omics + KG	0.8529 \pm 0.0153	0.8794 \pm 0.0114	0.8048 \pm 0.0541	0.7905 \pm 0.0436	0.8222 \pm 0.0347	0.8778 \pm 0.0192
G-Retriever + pre-GAT	0.8550 \pm 0.0046	0.8804 \pm 0.0037	0.8524 \pm 0.0165	0.8857 \pm 0.0000	0.8667\pm0.0000	0.8667 \pm 0.0000
GALAX	0.8815\pm0.0033	0.9249\pm0.0048	0.8810\pm0.0082	0.9238\pm0.0436	0.8500 \pm 0.0441	0.8889\pm0.0839

Baselines and Ablation Study Traditional method, M2T (Multiomic2Target(Deng et al., 2024)), serves as a baseline that uses only multi-omic features without graph or language modeling and performs poorly across all metrics. And we perform ablation studies to isolate the contribution of core components of language and graph modules in GALAX. On the language axis, a non-task-tuned LLaMA3 (L3+Omics) is weak; domain-adaptive finetuning on biomedical text (L3-FT(Med)+Omics) yields modest gains; task-adaptive finetuning on Target-QA (L3-

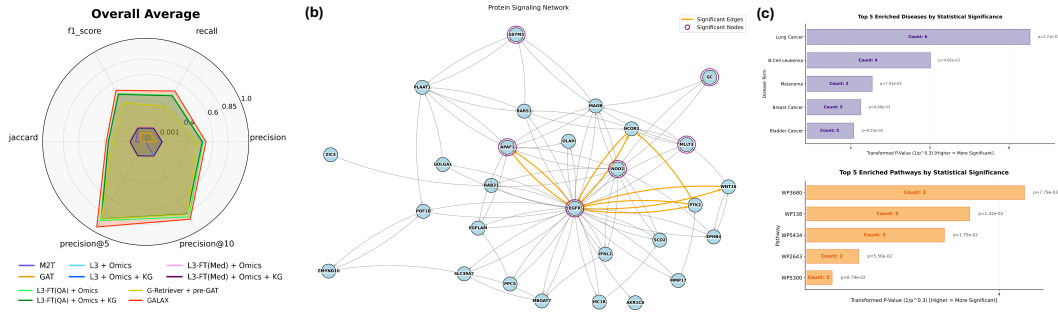


Figure 4: Model performance and analysis. (a) Overall performance across metrics. (b) LUAD (ACH-000860): cancer-relevant subgraph highlighting disease-associated nodes (purple) and enrichment-supported edges (orange). (c) Enrichment analysis: top pathway and disease terms with p -values and gene counts.

FT(QA)+Omic) produces the step-change. On the graph axis, **GAT** incorporates graph foundation model and trained to predict the CRISPR knockout effects, shows limited improvements. Furthermore, integrating graph modules into language models with different outputs. Adding a static KG to each language foundation models (**L3 / L3-FT(Med) / L3-FT(QA)+Omic+KG**) barely improve or even decrease model performances, and graph retrieval with pretrained GAT (**G-Retriever+pre-GAT**) outperform some task-adaptive finetuned language models but not reliably due to the difficulty of extracting relevant subgraphs from millions of nodes/edges. Reinforcement-guided subgraph construction on top of QA-tuned language (**GALAX: L3-FT(QA)+KG+RL**) delivers consistent, cross-dataset gains of roughly 2%-5% on each metric, indicating that a reinforcement-guided subgraph generator outperforms other graph augmented models across all datasets by enabling process-level reasoning over biologically plausible subgraphs, and that QA finetuning provides the dominant improvement (shown in Tables 1–2). Full baseline and ablation results are provided in Appendix D.3.

Computational Complexity We denote the language model complexity as $O(\kappa)$. The retrieved KG subgraph contains M nodes, and ε denotes graph embedding cost. Augmented with KG retrieval, L3-FT(QA)+Omic+KG adds $O(M^2)$ per query and results in $O(\kappa + M^2\varepsilon)$ for training and inference. G-retriever+preGAT embed M nodes, requiring $O(M\varepsilon + M^2\varepsilon)$, thus $O(\kappa + M\varepsilon + M^2\varepsilon)$ for training and inference. GALAX augments language model with reinforcement-guided subgraph construction, whose embedding costs $O(M\varepsilon + M^2\varepsilon)$. The LLM demands an $O(\kappa)$ initialization for the top η candidates and the same for final answer generation; since $\eta \ll M$, graph embedding dominates the reward term in the RL cost. Consequently, the overall training and inference complexity is $O(\kappa + M\varepsilon + M^2\varepsilon)$ (see Table 3).

Model	Training & Inference
L3-FT(QA)+Omic	$O(\kappa)$
L3-FT(QA)+Omic+KG	$O(\kappa + M^2)$
G-retriever+preGAT	$O(\kappa + M\varepsilon + M^2\varepsilon)$
GALAX	$O(\kappa + M\varepsilon + M^2\varepsilon)$

Table 3: Complexity comparisons

Main Results Table 1 summarizes the performance of GALAX and several competitive baselines across the full test dataset, with LUAD and BRCA representing the cancer types with the largest sample sizes in Target-QA. GALAX significantly outperforms all baselines on every evaluation metric. For example, it achieves an overall precision of **0.5472** and recall of **0.5332**, exceeding the strongest baseline L3-FT(QA) + Omic in both metrics. The model also demonstrates strong performance across LUAD, BRCA, and other cancer-specific subsets, highlighting its robustness and generalizability. To further assess the quality of target prioritization, we evaluate Hit@10 and Hit@5, as shown in Table 2. GALAX achieves the highest accuracy across most evaluation settings, with an overall Hit@10 of **0.8815** and Hit@5 of **0.9249**. Figure 4b-c illustrates the explainable subgraph generated for the lung cancer cell line ACH-000860. To further validate the biological relevance of the extracted subgraph, we performed functional enrichment analysis. The results reveal significant enrichment in cancer-associated signaling pathways, including the cancer pathway WP5434 and EGFR-related receptor signaling pathways such as WP138 and WP3680, as cataloged in WikiPathways (Agrawal et al., 2024). Notably, EGFR a well-established therapeutic target in NSCLC (Steuer & Ramalingam, 2015) appears in five enriched terms, together with PTK2 and WNT16 which are known to regulate invasion, epithelial mesenchymal transition, and therapeutic resistance (Tong et al., 2019; Sun et al., 2012). The observed pathway enrichment provides strong biological support for the relevance of the selected targets in lung cancer. Additional disease enrichment using the GAD DISEASE database further supports this conclusion (Sherman et al., 2022),

with lung cancer identified as the top associated disease term with a p value of 0.0022, involving GSTM3, APAF1, NOD2, MLLT3, GC and EGFR. Full enrichment details across all cancer types are included in the Appendix D.4.

6 CONCLUSION

We present **GALAX**, a graph-augmented language model that integrates large language models with pretrained graph neural networks under the guidance of a Graph Process Reward Model (GPRM) to enable target prioritization through explainable subgraph reasoning. GALAX constructs subgraphs in a step-wise manner via reinforcement learning, using pretrained GNNs to evaluate the biological plausibility of each step—removing the need for intermediate annotations. This framework supports structured, clinically grounded reasoning over multi-omic data. To facilitate evaluation, we introduce **Target-QA**, a benchmark dataset integrating multi-omics and CRISPR outcomes. GALAX achieves performance gains over baselines across most evaluation metrics on Target-QA.

ETHICS STATEMENT

This dataset is derived from the Broad Institute’s Cancer Dependency Map (DepMap³) and will be released strictly for non-commercial, internal research and academic use, consistent with DepMap’s Terms of Use. We do not redistribute original DepMap files; instead, we provide derived, non-identifiable annotations and processing scripts/pointers so users can obtain the source data directly from DepMap after accepting its terms. The dataset is not intended for clinical applications and must not be used for any Commercial Use (e.g., direct sale, incorporation into a product, or training/developing/enhancing ML/AI models beyond internal academic research). Users agree to acknowledge DepMap and the Broad Institute using the acknowledgement wording specified by DepMap, and to respect any third-party rights that may attach to the underlying data. Users must preserve confidentiality and refrain from any re-identification attempts. This statement summarizes our compliance posture and does not constitute legal advice; users are responsible for ensuring their own compliance with DepMap’s Terms and applicable policies.

REPRODUCIBILITY STATEMENT

We release the source code of **GALAX**⁴ in GitHub, together with preprocessing pipelines, thereby enabling reproduction of Target-QA datasets and reported experiments. **Target-QA**⁵ dataset is also available in Huggingface.

REFERENCES

- Josh Achiam, Steven Adler, Sandhini Agarwal, Lama Ahmad, Ilge Akkaya, Florencia Leoni Aleman, Diogo Almeida, Janko Altenschmidt, Sam Altman, Shyamal Anadkat, et al. Gpt-4 technical report. *arXiv preprint arXiv:2303.08774*, 2023.
- Ayushi Agrawal, Hasan Balci, Kristina Hanspers, Susan L Coort, Marvin Martens, Denise N Slenter, Friederike Ehrhart, Daniela Digles, Andra Waagmeester, Isabel Wassink, et al. Wikipathways 2024: next generation pathway database. *Nucleic acids research*, 52(D1):D679–D689, 2024.
- AI@Meta. Llama 3 model card. 2024. URL https://github.com/meta-llama/llama3/blob/main/MODEL_CARD.md.
- Ricard Argelaguet, Britta Velten, Damien Arnol, Sascha Dietrich, Thorsten Zenz, John C Marioni, Florian Buettner, Wolfgang Huber, and Oliver Stegle. Multi-omics factor analysis—a framework for unsupervised integration of multi-omics data sets. *Molecular systems biology*, 14(6):e8124, 2018.
- Yuntao Bai, Andy Jones, Kamal Ndousse, Amanda Askell, Anna Chen, Nova DasSarma, Dawn Drain, Stanislav Fort, Deep Ganguli, Tom Henighan, et al. Training a helpful and harmless assistant with reinforcement learning from human feedback. *arXiv preprint arXiv:2204.05862*, 2022.

³DepMap: <https://depmap.org/portal/>

⁴GitHub: <https://github.com/FuhaiLiAiLab/GALAX>

⁵Hugging Face: <https://huggingface.co/datasets/FuhaiLiAiLab/Target-QA>

- Tom Brown, Benjamin Mann, Nick Ryder, Melanie Subbiah, Jared D Kaplan, Prafulla Dhariwal, Arvind Neelakantan, Pranav Shyam, Girish Sastry, Amanda Askell, et al. Language models are few-shot learners. *Advances in neural information processing systems*, 33:1877–1901, 2020.
- Francis Crick. Central dogma of molecular biology. *Nature*, 227(5258):561–563, 1970.
- JM Dempster, J Rossen, M Kazachkova, J Pan, G Kugener, DE Root, and A Tsherniak. Extracting biological insights from the project achilles genome-scale crispr screens in cancer cell lines. *bioRxiv*. 2019: 720243. DOI: <https://doi.org/10.1101/720243>.
- Eden Z Deng, Giacomo B Marino, Daniel JB Clarke, Ido Diamant, Adam C Resnick, Weiping Ma, Pei Wang, and Avi Ma’ayan. Multiomics2targets identifies targets from cancer cohorts profiled with transcriptomics, proteomics, and phosphoproteomics. *Cell Reports Methods*, 4(8), 2024.
- Bahare Fatemi, Jonathan Halcrow, and Bryan Perozzi. Talk like a graph: Encoding graphs for large language models. *arXiv preprint arXiv:2310.04560*, 2023.
- Leo Gao, John Schulman, and Jacob Hilton. Scaling laws for reward model overoptimization. In *International Conference on Machine Learning*, pp. 10835–10866. PMLR, 2023.
- Yehudit Hasin, Marcus Seldin, and Aldons Lusic. Multi-omics approaches to disease. *Genome biology*, 18:1–15, 2017.
- Xiaoxin He, Yijun Tian, Yifei Sun, Nitesh Chawla, Thomas Laurent, Yann LeCun, Xavier Bresson, and Bryan Hooi. G-retriever: Retrieval-augmented generation for textual graph understanding and question answering. *Advances in Neural Information Processing Systems*, 37:132876–132907, 2024.
- Tomasz Korbak, Kejian Shi, Angelica Chen, Rasika Vinayak Bhalerao, Christopher Buckley, Jason Phang, Samuel R Bowman, and Ethan Perez. Pretraining language models with human preferences. In *International Conference on Machine Learning*, pp. 17506–17533. PMLR, 2023.
- Vessela N Kristensen, Ole Christian Lingjærde, Hege G Russnes, Hans Kristian M Vollan, Arnoldo Frigessi, and Anne-Lise Børresen-Dale. Principles and methods of integrative genomic analyses in cancer. *Nature Reviews Cancer*, 14(5):299–313, 2014.
- Jinhyuk Lee, Wonjin Yoon, Sungdong Kim, Donghyeon Kim, Sunkyu Kim, Chan Ho So, and Jaewoo Kang. Biobert: a pre-trained biomedical language representation model for biomedical text mining. *Bioinformatics*, 36(4):1234–1240, 2020.
- Brian Lester, Rami Al-Rfou, and Noah Constant. The power of scale for parameter-efficient prompt tuning. *arXiv preprint arXiv:2104.08691*, 2021.
- Patrick Lewis, Ethan Perez, Aleksandra Piktus, Fabio Petroni, Vladimir Karpukhin, Naman Goyal, Heinrich Küttler, Mike Lewis, Wen-tau Yih, Tim Rocktäschel, et al. Retrieval-augmented generation for knowledge-intensive nlp tasks. *Advances in neural information processing systems*, 33: 9459–9474, 2020.
- Tianxiang Li, Yanyan Yang, Hongzhao Qi, Weigang Cui, Lin Zhang, Xiuxiu Fu, Xiangqin He, Meixin Liu, Pei-Feng Li, and Tao Yu. CRISPR/Cas9 therapeutics: progress and prospects. *Signal Transduct. Target. Ther.*, 8(1):36, January 2023.
- Xiao Li, Jie Ma, Ling Leng, Mingfei Han, Mansheng Li, Fuchu He, and Yunping Zhu. Mogcn: a multi-omics integration method based on graph convolutional network for cancer subtype analysis. *Frontiers in Genetics*, 13:806842, 2022.
- Hunter Lightman, Vineet Kosaraju, Yuri Burda, Harrison Edwards, Bowen Baker, Teddy Lee, Jan Leike, John Schulman, Ilya Sutskever, and Karl Cobbe. Let’s verify step by step. In *The Twelfth International Conference on Learning Representations*, 2023.
- Liangchen Luo, Yinxiao Liu, Rosanne Liu, Samrat Phatale, Harsh Lara, Yunxuan Li, Lei Shu, Yun Zhu, Lei Meng, Jiao Sun, et al. Improve mathematical reasoning in language models by automated process supervision, 2024. URL <https://arxiv.org/abs/2406.6592>.

- Linhao Luo, Yuan-Fang Li, Gholamreza Haffari, and Shirui Pan. Reasoning on graphs: Faithful and interpretable large language model reasoning. *arXiv preprint arXiv:2310.01061*, 2023.
- Chen Meng, Oana A Zeleznik, Gerhard G Thallinger, Bernhard Kuster, Amin M Gholami, and Aedín C Culhane. Dimension reduction techniques for the integrative analysis of multi-omics data. *Briefings in bioinformatics*, 17(4):628–641, 2016.
- Nam D Nguyen and Daifeng Wang. Multiview learning for understanding functional multiomics. *PLoS computational biology*, 16(4):e1007677, 2020.
- OpenAI. Chatgpt: Mar 14 version. <https://chat.openai.com/>, 2023. Accessed: 2025-05-15.
- Xubin Ren, Jiabin Tang, Dawei Yin, Nitesh Chawla, and Chao Huang. A survey of large language models for graphs. In *Proceedings of the 30th ACM SIGKDD Conference on Knowledge Discovery and Data Mining*, pp. 6616–6626, 2024.
- Florian Rohart, Benoît Gautier, Amrit Singh, and Kim-Anh Lê Cao. mixomics: An r package for ‘omics feature selection and multiple data integration. *PLoS computational biology*, 13(11): e1005752, 2017.
- John Schulman, Filip Wolski, Prafulla Dhariwal, Alec Radford, and Oleg Klimov. Proximal policy optimization algorithms. *arXiv preprint arXiv:1707.06347*, 2017.
- Ophir Shalem, Neville E Sanjana, Ella Hartenian, Xi Shi, David A Scott, Tarjei S Mikkelsen, Dirk Heckl, Benjamin L Ebert, David E Root, John G Doench, et al. Genome-scale crispr-cas9 knock-out screening in human cells. *Science*, 343(6166):84–87, 2014.
- Zhihong Shao, Peiyi Wang, Qihao Zhu, Runxin Xu, Junxiao Song, Xiao Bi, Haowei Zhang, Mingchuan Zhang, YK Li, Y Wu, et al. Deepseekmath: Pushing the limits of mathematical reasoning in open language models. *arXiv preprint arXiv:2402.03300*, 2024.
- Ronglai Shen, Adam B Olshen, and Marc Ladanyi. Integrative clustering of multiple genomic data types using a joint latent variable model with application to breast and lung cancer subtype analysis. *Bioinformatics*, 25(22):2906–2912, 2009.
- Brad T Sherman, Ming Hao, Ju Qiu, Xiaoli Jiao, Michael W Baseler, H Clifford Lane, Tomozumi Imamichi, and Weizhong Chang. David: a web server for functional enrichment analysis and functional annotation of gene lists (2021 update). *Nucleic acids research*, 50(W1):W216–W221, 2022.
- Junwei Shi, Eric Wang, Joseph P Milazzo, Zihua Wang, Justin B Kinney, and Christopher R Vakoc. Discovery of cancer drug targets by crispr-cas9 screening of protein domains. *Nature biotechnology*, 33(6):661–667, 2015.
- Conor E Steuer and Suresh S Ramalingam. Targeting egfr in lung cancer: Lessons learned and future perspectives. *Molecular aspects of medicine*, 45:67–73, 2015.
- Sandra Steyaert, Marija Pizurica, Divya Nagaraj, Priya Khandelwal, Tina Hernandez-Boussard, Andrew J. Gentles, and Olivier Gevaert. Multimodal data fusion for cancer biomarker discovery with deep learning. *Nature Machine Intelligence*, 5(4):351–362, Apr 2023. ISSN 2522-5839. doi: 10.1038/s42256-023-00633-5. URL <https://doi.org/10.1038/s42256-023-00633-5>.
- Yu Sun, Judith Campisi, Celestia Higano, Tomasz M Beer, Peggy Porter, Ilsa Coleman, Lawrence True, and Peter S Nelson. Treatment-induced damage to the tumor microenvironment promotes prostate cancer therapy resistance through wnt16b. *Nature medicine*, 18(9):1359–1368, 2012.
- Xuexia Tong, Ryosuke Tanino, Rong Sun, Yukari Tsubata, Tamio Okimoto, Mayumi Takechi, and Takeshi Isobe. Protein tyrosine kinase 2: a novel therapeutic target to overcome acquired egfr-tyr resistance in non-small cell lung cancer. *Respiratory Research*, 20:1–14, 2019.

- Eric J. Topol. High-performance medicine: the convergence of human and artificial intelligence. *Nature Medicine*, 25(1):44–56, Jan 2019. ISSN 1546-170X. doi: 10.1038/s41591-018-0300-7. URL <https://doi.org/10.1038/s41591-018-0300-7>.
- Jonathan Uesato, Nate Kushman, Ramana Kumar, Francis Song, Noah Siegel, Lisa Wang, Antonia Creswell, Geoffrey Irving, and Irina Higgins. Solving math word problems with process-and outcome-based feedback. *arXiv preprint arXiv:2211.14275*, 2022.
- Petar Veličković, Guillem Cucurull, Arantxa Casanova, Adriana Romero, Pietro Lio, and Yoshua Bengio. Graph attention networks. *arXiv preprint arXiv:1710.10903*, 2017.
- Lei Wang, Wanyu Xu, Yihuai Lan, Zhiqiang Hu, Yunshi Lan, Roy Ka-Wei Lee, and Ee-Peng Lim. Plan-and-solve prompting: Improving zero-shot chain-of-thought reasoning by large language models. *arXiv preprint arXiv:2305.04091*, 2023.
- Tongxin Wang, Wei Shao, Zhi Huang, Haixu Tang, Jie Zhang, Zhengming Ding, and Kun Huang. Mogonet integrates multi-omics data using graph convolutional networks allowing patient classification and biomarker identification. *Nature communications*, 12(1):3445, 2021.
- Jason Wei, Xuezhi Wang, Dale Schuurmans, Maarten Bosma, Fei Xia, Ed Chi, Quoc V Le, Denny Zhou, et al. Chain-of-thought prompting elicits reasoning in large language models. *Advances in neural information processing systems*, 35:24824–24837, 2022.
- John N Weinstein, Eric A Collisson, Gordon B Mills, Kenna R Shaw, Brad A Ozenberger, Kyle Ellrott, Ilya Shmulevich, Chris Sander, and Joshua M Stuart. The cancer genome atlas pan-cancer analysis project. *Nature genetics*, 45(10):1113–1120, 2013.
- Heming Zhang, Yixin Chen, Philip Payne, and Fuhai Li. Using deepsignalingflow to mine signaling flows interpreting mechanism of synergy of cocktails. *npj Systems Biology and Applications*, 10(1):92, 2024a.
- Heming Zhang, Shunning Liang, Tim Xu, Wenyu Li, Di Huang, Yuhan Dong, Guangfu Li, J Philip Miller, S Peter Goedegebuure, Marco Sardiello, et al. Biomedgraphica: An all-in-one platform for biomedical prior knowledge and omic signaling graph generation. *bioRxiv*, 2024b.
- Heming Zhang, Tim Xu, Dekang Cao, Shunning Liang, Lars Schimmelpfennig, Levi Kaster, Di Huang, Carlos Cruchaga, Guangfu Li, Michael Province, et al. Omnicelltosg: The first cell text-omic signaling graphs dataset for joint llm and gnn modeling. *arXiv preprint arXiv:2504.02148*, 2025a.
- Jingyi Zhang, Jiaying Huang, Huanjin Yao, Shunyu Liu, Xikun Zhang, Shijian Lu, and Dacheng Tao. R1-vl: Learning to reason with multimodal large language models via step-wise group relative policy optimization. *arXiv preprint arXiv:2503.12937*, 2025b.

A THE USE OF LARGE LANGUAGE MODELS

We used ChatGPT-5 as a writing assistant. All LLM-suggested text was reviewed, fact-checked, and edited by the authors, who take full responsibility for the final content. The LLM is not an author and is not eligible for authorship under the ICLR Code of Ethics.

B DATASET

B.1 BIOMEDICAL TERMINOLGY CORPUS

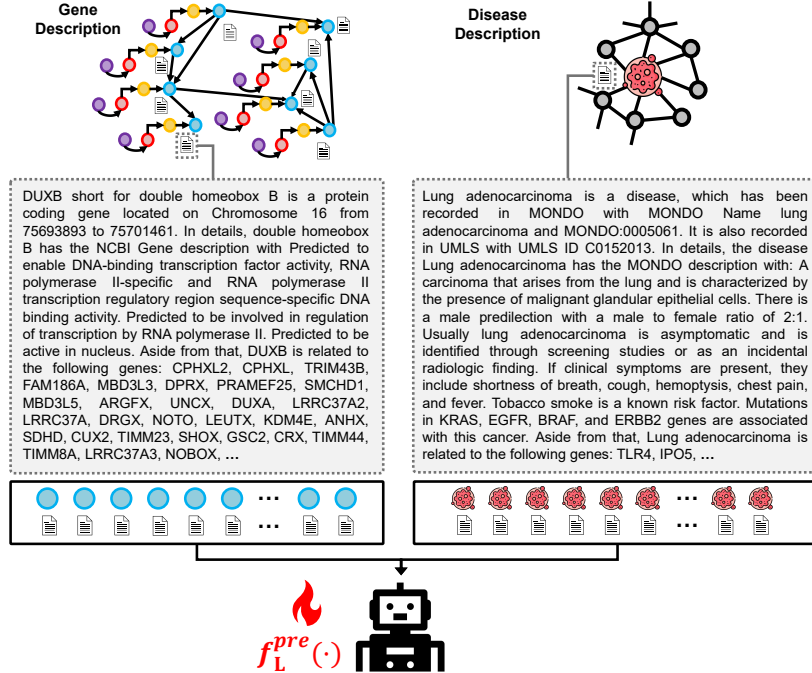


Figure 5: Biomedical Corpus Composition. Pretraining LLM $f_L^{\text{pre}}(\cdot)$ on biomedical terminology and structural patterns using protein-protein and disease-protein interactions.

Each entities or nodes in TOSG has the name and description about it with $\mathcal{T} = \{T_{\text{name}}, T_{\text{desc}}\}$, where $|T_{\text{name}}| = |T_{\text{desc}}| = M$. And disease entity has has an associated name and textual description with $\mathcal{S} = \{S_{\text{name}}, S_{\text{desc}}\}$ where $|\mathcal{S}| = M^{(S)}$. In the Figure 5, we pretrained f_L^{pre} with curated text copora in BioMedGraphica⁶, where they provided the data collection and integration source code. Following their processed descriptions, we incorporate $\mathcal{G}^{(\text{PPI})}$ and $\mathcal{G}^{(\text{DTI})}$ to enrich the corpus by appending protein-protein (PPI) and disease-protein (DTI) interaction information as textual descriptions after each protein and disease entity. For entities without known interactions, we assign empty strings during corpus construction, resulting in the intermediate representations \mathcal{T} and \mathcal{S} . In practice, we exclude these empty entities to derive the final input sets \mathcal{T}' and \mathcal{S}' , where $|\mathcal{T}'|$ includes 42,224 protein descriptions and \mathcal{S}' includes 22,340 disease descriptions (i.e., $|\mathcal{T}'| = 42,224$ and $|\mathcal{S}'| = M'^{(S)} = 22,340$). This yields a combined corpus of 64,564 text samples for pretraining.

B.2 DEPMAP DATA PREPROCESSING

As shown in Figure 6a, after multi-omics integration in BioMedGraphica of DepMap cohort (see Table 4) comprises $N^{(0)}$ ($N^{(0)} = 985$) cell-line samples, which are organized into three datasets: a pretraining set, Target-QA, and Drug-QA. Of these 985 samples, 336 samples lack disease/tcga-code annotations or belong to non-cancerous samples, while 649 samples cancerous. Within the annotated cancer set, 363 samples overlap with DepMap CRISPR multi-omic data. Since we would like to utilize as many as samples for training GALAX, we set $N = 363$ as Target-QA, $N^{(0)} = 336$

⁶<https://github.com/FuhaiLiAiLab/BioMedGraphica>

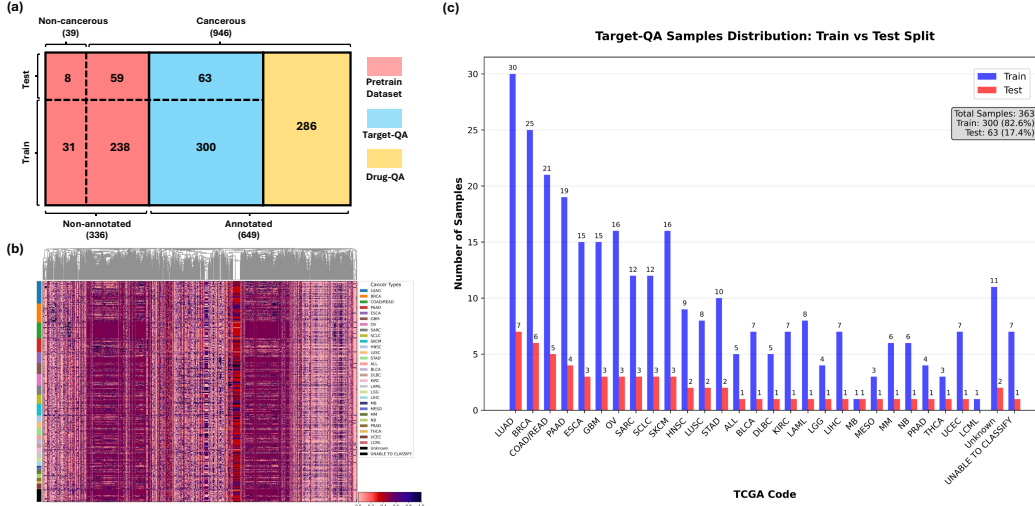


Figure 6: Dataset composition, feature landscape, and split statistics. (a) Block diagram of the corpus partitioned by phenotype (non-cancerous vs. cancerous) and by task: pretraining pool (pink), Target-QA (blue), and Drug-QA (yellow). Numbers within boxes denote sample counts; the dashed horizontal line marks the train/test division and the dashed vertical line marks the non-cancerous/cancerous and non-annotated/annotated boundaries. (b) Heatmap of standardized multi-omic features (top 5,000 most variance features) for Target-QA samples. Rows are samples (annotated by TCGA cancer type); columns are features with top variances. The colored sidebar encodes TCGA cancer types (legend at right). (c) Distribution of Target-QA samples by TCGA code for train (blue) and test (red); totals shown in the inset ($N = 363$; train = 300 (82.6%), test = 63 (17.4%)).

as pretraining set. To pretrain the graph foundation model, f_G^{pre}, f_G , we consider $|\mathcal{O}| = 2$ classes—cancerous (297 samples) and non-cancerous (39 samples)—and perform an 80/20 random split, yielding 269 training samples (238 cancerous, 31 non-cancerous) and 67 test samples (59 cancerous, 8 non-cancerous). The raw omics feature matrices include promoter and gene modalities $m^{(pm)}$ and $m^{(g)}$ (each with 86,238 entities), a transcript modality $m^{(t)}$ (412,039 transcript-level entities), and a protein modality $m^{(p)}$ (121,419 protein-level entities). The promoter modality is represented as a virtual node type in the graph encoder—entity-wise duplicates of genes whose omic values are drawn from DepMap methylation. Together, these modalities yield $M = 834,809$ omics entities (see Table 5). The unified knowledge graph integrates protein–protein interactions ($|\mathcal{E}| = 27,087,971$) and disease–target associations ($|\mathcal{E}^{(\text{PPI})}| = 17,151,453$). Every node in the Text-Omic Signaling Graph (TOSG) carries text attributes $\mathcal{T} = \{T_{\text{name}}, T_{\text{desc}}\}$ with $|T_{\text{name}}| = |T_{\text{desc}}| = M$; empty fields are set to the empty string to preserve schema alignment. Hence, we construct the TOSG by linking multi-omics features with biomedical relational knowledge using BioMedGraphica and pretrain the graph encoder f_G^{pre}, f_G (parameters $\theta_G^{\text{pre}}, \theta_G$) with a masked-edge modeling objective that encourages recovery of held-out interactions from context, capturing implicit omic relationships and signaling dependencies.

B.3 TARGET-QA GENERATION

Based on the raw data provided from the DepMap CRISPR gene effect data with 1178 samples, we get the overlapped 363 ($N = 363$) samples with the pretraining samples. And we do 80/20 train/test split with 80/20 ratio for 300 training samples and 63 test samples at random seeds. In total, we collected test samples from LUAD (7 samples), BRCA (6 samples), COAD/READ (5 samples), PAAD (4 samples), ESCA (3 samples), GBM (3 samples), OV (3 samples), SARC (3 samples), SCLC (3 samples), SKCM (3 samples), HNSC (2 samples), LUSC (2 samples), STAD (2 samples), etc. (see Figure 6C). Given that methylation values in DepMap have so many are 1 (full methylated over the promoter region around the transcription start site), which means that many values are ranked as top K ($K=10$), so we just omit the methylation (epigenomic) values by only providing genomic, transcriptomic and proteomic values. Afterwards, each QA sample is indexed by a unique key corresponding to the cancer cell line, such as:

- ACH-000098: The identifier for a glioblastoma cancer cell line.

Table 4: Descriptions and sources of raw data files used in this study

File Type	File Name	Download Site
Promoter feature	CCLE_RRBS_TSS1kb_20181022.txt	https://depmap.org/portal/data_page/?tab=allData
Gene feature	OmicsCNGene.csv	https://depmap.org/portal/data_page/?tab=allData
Transcript feature	See footnote [†]	https://depmap.org/portal/data_page/?tab=allData
Protein feature	protein_quant_current_normalized.csv	https://depmap.org/portal/data_page/?tab=allData
CRISPR gene effect	CRISPRGeneEffect.csv	https://depmap.org/portal/data_page/?tab=allData
Cell line annotation	Table_S1_Sample_Information.xlsx	https://depmap.org/portal/data_page/?tab=allData
Cell line annotation	cellosaurus.obo	https://ftp.expasy.org/databases/cellosaurus/cellosaurus.obo
Cell line status	cell-lines-in-Non-Cancerous.csv	https://depmap.org/portal/context/Non-Cancerous

[†] Transcript file name: OmicsExpressionProteinCodingGenesTPMLogp1BatchCorrected.csv

Table 5: Summary of feature dimensions across omics and samples

Modality	Raw Matrix	Processed Matrix
Promoter	21,337 rows, 846 samples	86,238 entities, 985 samples
Gene	38,590 rows, 1,928 samples	86,238 entities, 985 samples
Transcript	19,138 rows, 1,672 samples	412,039 entities, 985 samples
Protein	12,755 rows, 378 samples	121,419 entities, 985 samples
Cell Line Annotation	1,019 samples	985 samples
Non-cancer Samples	137 samples	39 samples

The corresponding JSON object contains the following fields:

- **cell_line_name:** Name of the cancer cell line (e.g., GAMG).
- **sample_dti_index:** Index for omics numpy data to be fetched.
- **disease:** Name of the associated disease (e.g., glioblastoma).
- **disease_bmgc_id:** BioMedGraphica-Conn identifier of the disease (e.g., BMGC_DS00965).
- **input:**
 - **top_k_gene, top_k_transcript, top_k_protein:**
 - * hgnc_symbols: List of gene/transcript/protein names.
 - * protein_bmgc_ids: Corresponding BioMedGraphica-Conn identifiers.
 - * protein_llmname_ids: Other synonymy names or IDs for corresponding genes/transcripts/proteins.
 - **knowledge_graph:**
 - * disease_protein: Includes bmgc_ids, hgnc_symbols, and indices for disease-associated proteins.

- * `ppi_neighbors`: PPI-linked proteins with similar structure as above.
- * `protein_relationships`: Textual descriptions of biological interactions (e.g., "BRCA1 → TP53").
- **ground_truth_answer**: Contains the validated target(s) used for evaluation:
 - `hgnc_symbols`: HGCN symbol names for CRISPR targets
 - `protein_bmgc_ids`: Corresponded CRISPR targets names for BioMedGraphica-Conn names
 - `protein_llmname_ids`: Other synonymy names or IDs

This hierarchical structure supports multi-modal reasoning by organizing omic features, biomedical knowledge graphs, and ground-truth target labels, where the cell line name is denoted as c_n , the disease name as s'_n , the top-ranked genes, transcripts, and proteins as $X_n^{(K)}$, and the associated knowledge graph as $\mathcal{G}_n^{(\text{sub})}$.

C PRETRAINING OF FOUNDATION MODELS

C.1 LLM PRETRAINING ON BIOMEDICAL CORPUS

We pretrain a large language model, denoted as f_L^{pre} with parameters θ_L^{pre} , using curated text corpora from final input sets \mathcal{T}' and \mathcal{S}' . Hence, by pretraining the Llama3-8B-Instruct for 3 epochs using a per-device batch size of 16 and a gradient accumulation step of 8, resulting in an effective batch size of 128. The optimizer was AdamW with a learning rate of $1e-5$, no weight decay, and a cosine learning rate schedule with a warm-up ratio of 10%. Gradient clipping was applied with a maximum gradient norm of 1.0. To improve memory efficiency during training, we enabled gradient checkpointing and utilized `bf16` precision while disabling `fp16`. Training proceeded for 336 steps, with the loss decreasing from approximately 2.2 at the start to around 0.7 by the end (see Figure 7).

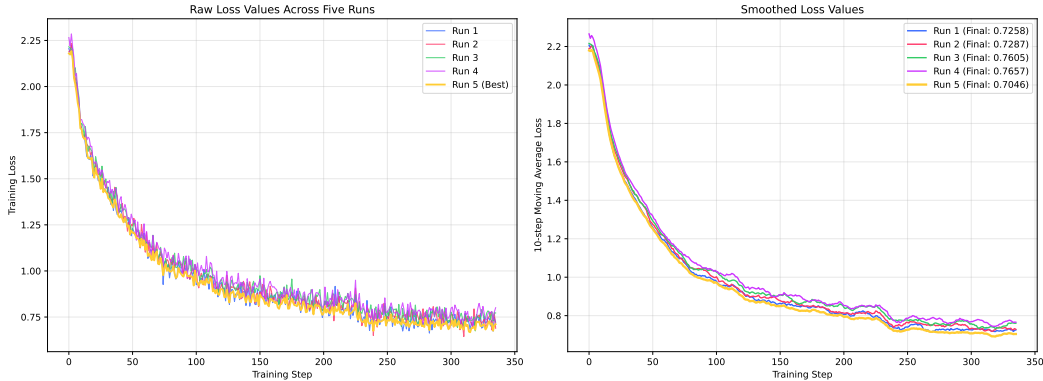


Figure 7: Pretraining language model loss on biomedical corpus

C.2 LLM PRETRAINING ON TARGET-QA

We will supervise the language model using the refined answer A_n as the ground-truth label from Target-QA with:

$$\mathcal{L}_{\text{init}} = - \sum_{n=1}^N \sum_{j=1}^J \log \xi_{\theta_{\text{init}}, \theta_L}(a_{n,j} | a_{n,<j}, P_n^{(\text{init})}) \quad (15)$$

, where $P_n^{(\text{init})}$ is the structured prompt as shown in Table 6. This objective enables the model to refine its initial answering based on user-specific and naive graph information. In details, for each sample c_n , a question is constructed as $Q_n = \{c_n, s'_n, X_n^{(K)}, \mathcal{G}_n^{(\text{sub})}\}$, which integrates the cell line identifier, disease label, multi-omics features, and a knowledge subgraph specific to the sample context. The corresponding answer A_n is a sentence that enumerates the top γ CRISPR-prioritized gene targets for sample n , denoted as $R_n = \{r_{n,1}, r_{n,2}, \dots, r_{n,\gamma}\}$. Each data instance is represented

Table 6: Prompt design for $P_n^{(\text{init})}$ and expected output for initial protein target reasoning.

Section	Content
Instruction	Identify the 100 priority genes whose knockout causes the strongest negative effect on the viability or proliferation of cell line c_n in the context of disease s'_n , based on multi-omics and knowledge graph signals.
Input	<ul style="list-style-type: none"> - Top 10 ranked genes with amplification from copy number data: $g_1^{(n)}, g_2^{(n)}, \dots, g_K^{(n)}$ - Top 10 ranked transcripts with high expression: $t_1^{(n)}, t_2^{(n)}, \dots, t_K^{(n)}$ - Top 10 ranked proteins from RPPA: $p_1^{(n)}, p_2^{(n)}, \dots, p_K^{(n)}$ - Disease-associated proteins from the knowledge graph: $\mathcal{V}_n^{(\text{sub})}$ - Known protein–protein/disease–protein relationships: $\mathcal{E}_n^{(\text{sub})}$
Output	<p>Based on the integrated multi-omics data and knowledge graph, I identified the 100 genes whose knockout is predicted to have the most severe negative impact on the viability or proliferation of the c_n cell line in s'_n. The prioritized gene list is as follows:</p> <ol style="list-style-type: none"> 1. $r_{n,1}^{(\text{init})}$ 2. $r_{n,2}^{(\text{init})}$ 3. $r_{n,3}^{(\text{init})}$... <p>These genes represent critical vulnerabilities for the given cell line under the disease context.</p>

as a tuple $D_n = (Q_n, A_n)$, and the full dataset is given by $\mathcal{D} = \{D_1, D_2, \dots, D_N\}$. The input to the model is a structured prompt $P_n^{(\text{init})}$ derived from Q_n , in which the knowledge subgraph $\mathcal{G}_n^{(\text{sub})}$ is translated into a natural language format designed for expert-level graph reasoning. For example, a subgraph $\mathcal{G}_n^{(\text{sub})}$ may contain nodes BRCA1, TP53, EGFR, MAPK1, AKT1, PIK3CA, MTOR, PTEN, and CDK2, with observed interactions: BRCA1 \rightarrow TP53, TP53 \rightarrow EGFR, EGFR \rightarrow MAPK1, EGFR \rightarrow AKT1, AKT1 \rightarrow MTOR, PIK3CA \rightarrow AKT1, PIK3CA \rightarrow PTEN, PTEN \rightarrow MTOR, and MAPK1 \rightarrow CDK2. This subgraph defines the molecular context for reasoning about gene knockout effects in the cell line c_n under disease condition s'_n . We conduct five independent finetuning trials using the constructed Target-QA dataset, each initialized with a different random seed. The resulting training loss trajectories are shown in Figure 8. Among these, the best-performing run (run 5) exhibits stable convergence, beginning with an initial loss of approximately 1.3 and reaching a final loss of around 0.3. We select this run as the final model checkpoint and designate it as our initial model f_{init} , which serves as the foundation for downstream reasoning and refined target prioritization.

For pretraining f_{init} with parameterized θ_{init} , we pretrain for 5 epochs with per-device batch size 1 and gradient accumulation 2 (effective global batch size = $2 \times \text{GPUs}$), using AdamW (`adamw_torch`) with learning rate 1×10^{-5} , cosine schedule with 10% warmup, and gradient clipping at 0.5. We enable gradient checkpointing and `bf16` (with `fp16` disabled), run on $2 \times \text{NVIDIA H100 80GB}$ with DeepSpeed ZeRO-3. Checkpointing and evaluation occur every 67 steps with up to 5 checkpoints retained. Data loading uses 4 workers, pinned memory, no last-batch drop, and no length grouping; we set `seed=42`.

C.3 GRAPH FOUNDATION MODELS

Pretraining for Capturing the Edge Mechanism We pretrain a graph model, denoted as f_G^{pre} with parameters θ_G^{pre} , using pretraining samples from $\mathcal{X}^{(0)}$. To effectively model graph-structured biological relationships, we pretrain our model using a masked edge prediction objective combined with random walk-based graph sampling. The process starts by masking a small fraction ($p = 0.0001$) of edges, allowing the model to infer missing interactions based on surrounding omics and text-derived features. We adopt a GAT-based encoder with two layers, each consisting of 8 hidden channels. Decoder layers use 4 channels. Both encoder and decoder modules apply dropout at a rate of 0.2. The model supports optional batch normalization and uses a `leaky_relu`

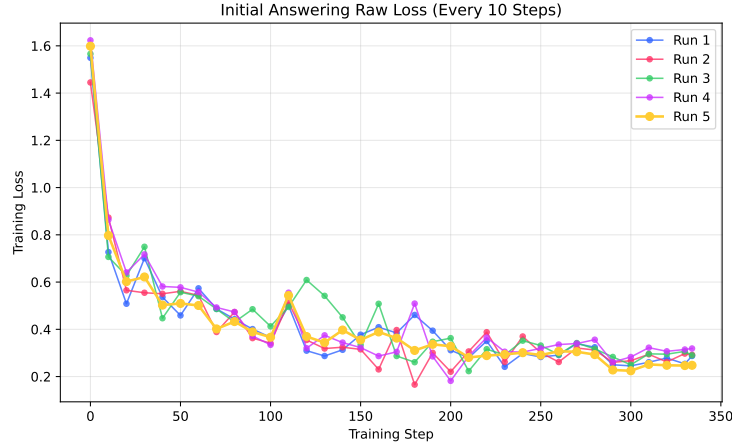


Figure 8: Initial language answering training loss

activation function. An internal encoder stack of up to 4 layers enables deeper relational modeling. All architecture and training options are managed through a reproducible `argparse` interface. Multimodal inputs include one omic feature and a text embedding of dimension 1, initialized using BioBERT v1.1. The model optionally supports training of the text encoder via `train_text`. We use a pretraining batch size of 4 for omics data and 64 for text. The optimizer is AdamW with a learning rate of 0.001, weight decay of 5×10^{-5} , and gradient norm clipping at 1.0.

The pretrained model is evaluated using average loss, AUC, and average precision (AP) over validation batches. As shown in Figure 9, the model demonstrates progressive improvement across steps, reaching a minimum batch loss of 0.140, peak AUC of 0.644, and peak AP of 0.619. These results confirm that the model successfully learns meaningful edge semantics and multimodal associations during pretraining. All training is conducted on a single NVIDIA H100 GPU (80GB).

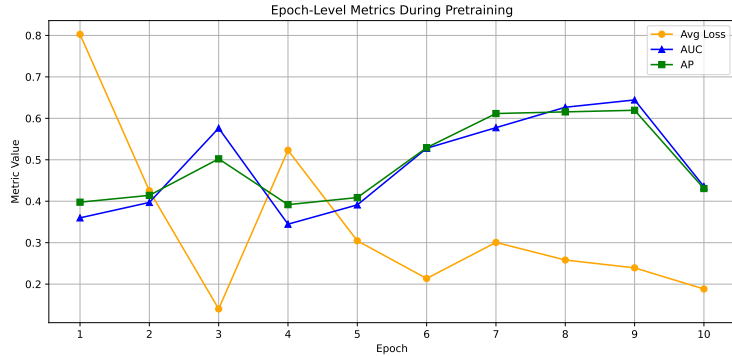


Figure 9: Pretraining loss to capture gene regulatory mechanism

Pretraining for Capturing the Cancerous Status Due to the severe class imbalance in the training set, we apply random oversampling to the minority class (non-cancerous) to balance the class distribution during the pretraining of the graph encoder f_G . We pretrained a Graph Attention Network (GAT) model f_G^{pre} with parameters θ_G^{pre} , and selected the best-performing checkpoint based on test accuracy. The selected model achieved a training loss of 0.036, training accuracy of 99.46%, and training F1 score of 0.996. On the test set, it obtained a loss of 0.370, accuracy of 96.15%, and F1 score of 0.973, demonstrating strong generalization to both classes.

D EXPERIMENT DETAILS

D.1 PROMPT AND CONTEXT DESIGN FOR FINETUNING

Same as aforementioned prompt design shown in Table 6, we construct the final-stage prompt $P_n^{(\text{final})}$, which incorporates both the initial answering and the subgraph-based regulatory context, as detailed in Table 7. We perform five additional finetuning trials using this refined prompt format.

Table 7: Refined prompt design for $P_n^{(\text{final})}$ and output with graph context

Section	Content
Instruction	Based on initial LLM reasoning and the subsignaling gene regulatory network identified by the subgraph generator, please identify the 100 priority genes whose knockout causes the strongest negative effect on the viability or proliferation of cell line c_n in the context of disease s'_n .
Input	<ul style="list-style-type: none"> - Top 10 ranked genes with amplification from copy number data: $g_1^{(n)}, \dots, g_K^{(n)}$ - Top 10 ranked transcripts with high expression: $t_1^{(n)}, \dots, t_K^{(n)}$ - Top 10 ranked proteins from RPPA: $p_1^{(n)}, \dots, p_K^{(n)}$ - Disease-associated proteins from the biomedical knowledge graph: $\mathcal{V}_n^{(\text{sub})}$ - Known protein-protein/disease-protein relationships: $\mathcal{E}_n^{(\text{sub})}$ - Identified Subsinging Gene Regulatory Network from Graph Generator <ul style="list-style-type: none"> - Involved genes in best connected subgraph: $\mathcal{V}_n^{(\text{conn})}$ - Inferred signaling cascade (edge text): $\mathcal{E}_n^{(\text{sub})}$
Refined Reasoning	<p>Based on the integrated multi-omics data and knowledge graph, I identified the 100 genes whose knockout is predicted to have the most severe negative impact on the viability or proliferation of the c_n cell line in s'_n. The prioritized gene list is as follows:</p> <ol style="list-style-type: none"> 1. $\hat{r}_{n,1}$ 2. $\hat{r}_{n,2}$ 3. $\hat{r}_{n,3}$... <p>These genes represent critical vulnerabilities for the given cell line under the disease context.</p>

The corresponding training are illustrated in Figure 10, where the best run (run 5) demonstrates smooth convergence and is selected as the final model checkpoint f_{final} for generating the ultimate target predictions.

D.2 HYPERPARAMETERS

For finetuning, the model is trained for 5 epochs with a per-device batch size of 1 and a gradient accumulation step of 2, resulting in an effective batch size of 2. We use the AdamW optimizer (`adamw_torch`) with a learning rate of 1×10^{-5} , no weight decay, and cosine learning rate scheduling with a 10% warm-up ratio. Gradient clipping is applied with a maximum gradient norm of 0.5. To support memory efficiency and large model training, we enable gradient checkpointing and use `bf16` precision (with `fp16` explicitly disabled). Training is accelerated using DeepSpeed Stage 3 parallelism, configured via an external JSON file. All experiments are conducted using 2 NVIDIA H100 GPUs, each with 80GB of memory. The DeepSpeed configuration enables ZeRO Stage 3 with both optimizer and parameter offloading to CPU, memory pinning, communication overlap, and gradient contiguity. Key parameters include automatic tuning of reduce bucket sizes and micro-batch size, sub-grouping disabled, and support for 16-bit weight gathering upon model saving. Gradient accumulation steps, clipping, learning rate, weight decay, and total training steps are all set to "auto" for adaptive scaling. Warmup is controlled via `WarmupDecayLR`, which adjusts the schedule based on total steps. Model checkpoints and evaluation are performed every 67 steps, with up to 5 checkpoints retained. Logging is performed at every step. For data loading, we use 4 dataloader workers and retain all batches (i.e., `drop_last=False`). Both the initial answering finetuning and second stage finetuning for f_{final} .

To generate high-quality and biologically reasonable subgraph explanations, we implement a reinforcement-guided generator, denoted as $\pi(\cdot)$, which operates over sample-specific graph states and candidate sets. To enhance robustness under noisy or unstable generation dynamics, we introduce a retry-based mechanism that adaptively tunes key hyperparameters with multiple runs ($\Omega = 6$, and ω denotes the current number of runs), dynamically adjusting the configuration to encourage exploration and improve convergence. Specifically, the number of training epochs is reduced from 5 to a minimum of 2, promoting faster reinitialization. Simultaneously, the learning

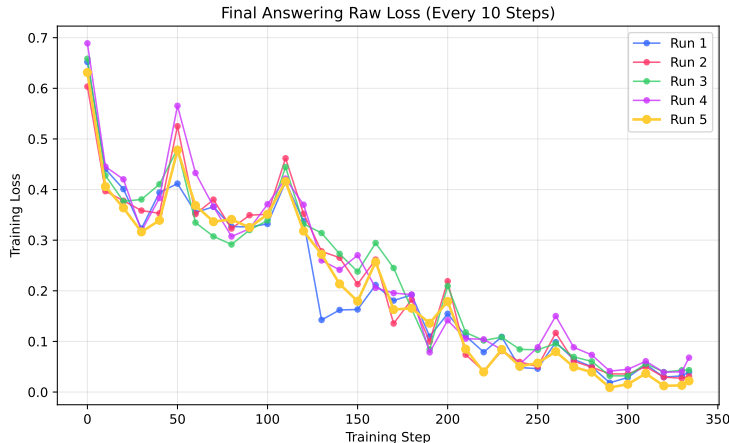


Figure 10: Final language answering training loss

rate is increased linearly from an initial value of 1×10^{-3} to $0.001 \cdot (1 + \omega)$ to escape local minima. The maximum number of nodes per graph is reduced from 200 to 100 in steps of 25. The maximum number of graph construction steps i per rollout is similarly reduced from 50 to 20 in steps of 5. The retry mechanism enables efficient navigation of the search space while preserving biological plausibility through domain-specific priors embedded in the reward formulation.

D.3 BASELINE MODELS

Multiomics2Target `Multiomics2Target`⁷ is a statistical and knowledge-based framework that integrates transcriptomics, proteomics, and phosphoproteomics to identify cancer-specific therapeutic targets. It leverages curated background knowledge databases and enrichment algorithms to compare tumor profiles against normal tissues, aiming to highlight targets uniquely activated in cancer. Specifically, the method filters out candidates that lack protein-level evidence or are not phosphorylated, and prioritizes those enriched in oncogenic pathways and subtype-specific signaling patterns. The workflow accounts for tumor heterogeneity by enabling both subtype-level and patient-specific analyses, thereby offering a safer and more context-aware target identification strategy. However, as a non-learning-based baseline, `Multiomics2Target` relies purely on statistical associations, which limits its precision in complex settings. As shown in the evaluation (see Figure 11), this method demonstrates poor performance compared to other approaches, failing to accurately prioritize the most effective targets. The model takes as input the cell line’s multi-omics features and outputs a ranked report of candidate targets, but its statistical scoring alone is insufficient to capture deeper, context-specific biological relevance.

GAT As a graph-based baseline, we adapt a Graph Attention Network (GAT) to assess the effect of gene knockouts using multi-omics data and CRISPR-derived gene effect scores. The input graph represents a biological hierarchy, where nodes correspond to genes, transcripts, and proteins, and edges capture central dogma relationships and known molecular interactions. For each gene of interest, we simulate the perturbation process by masking the node corresponding to the gene and recursively masking its downstream elements—namely its associated transcripts and translated proteins—mimicking the transcriptional and translational disruptions observed during a real gene knockout. This masked subgraph is then passed to the GAT model based on the pretrained model f_G^{pre} (parameterized by θ_G^{pre}), which aggregates information from the unmasked neighborhood to predict the impact of the knockout on cellular viability, matching the gene effect values from the CRISPR dataset. This design allows us to evaluate how well the local subgraph structure and omics context can recover the observed CRISPR perturbation effect. Although this method incorporates the biological topology and omics signals through attention-weighted message passing, it lacks explicit global reasoning for disease mechanism and has low performance on CRISPR target prediction.

G-Retriever G-Retriever is a graph language framework that enables conversational interaction with large, complex graphs enriched with textual node and edge attributes. It facilitates question

⁷<https://multiomics2targets.maayanlab.cloud/>

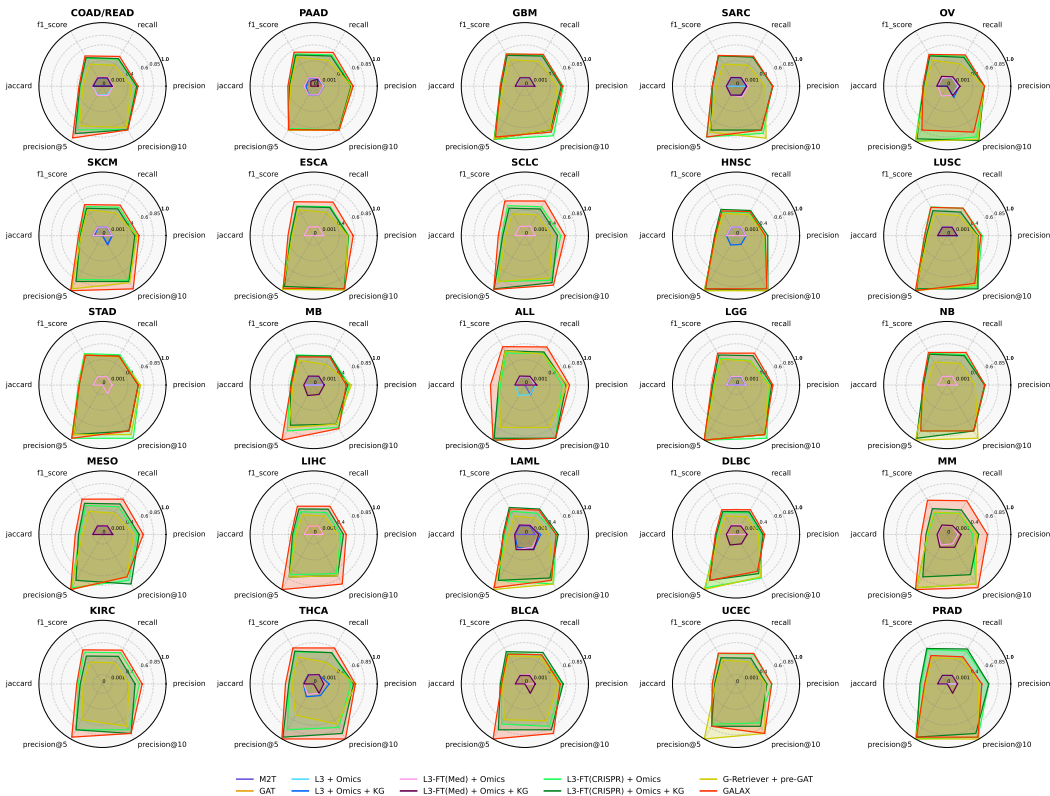


Figure 11: Model performance plots over main Target-QA datasets

answering by aligning user queries in natural language with the underlying graph structure, returning both textual responses and highlighted subgraph evidence. This setup is particularly useful for scenarios where graph elements (e.g., proteins, drugs, phenotypes) are associated with rich descriptions or biomedical annotations. In our implementation, we instantiate G-Retriever with two pretrained components: (1) a language model f_{init} that has been fine-tuned on domain-specific question-answering tasks—specifically, CRISPR-target-related biomedical questions; (2) a graph encoder based on a pretrained Graph Attention Network (GAT), denoted as f_G^{pre} , parameterized by θ_G^{pre} . The GAT is trained to encode signaling pathway graphs and capture topological and contextual dependencies between biological entities such as genes, proteins, and molecular interactions. This dual-modality initialization, textual reasoning via f_{init} and structural embedding via f_G^{pre} , allows G-Retriever to support context-aware retrieval over large graphs that exceed the LLM’s context window. Through this integration, the framework effectively aligns natural language queries with underlying graph structures, enabling biologically grounded reasoning over complex networks. While G-Retriever offers modest performance improvements over conventional GraphRAG baselines—particularly in terms of contextual relevance and retrieval accuracy—it remains limited in its ability to construct biologically interpretable subgraphs with strong explanatory power. Specifically, G-Retriever lacks a mechanism for enforcing structural coherence or pathway-level constraints, which are essential for generating subgraphs with high fidelity to known signaling or regulatory cascades. Consequently, its generated outputs often fall short of the domain-specific interpretability and performance achieved by our proposed method, which integrates graph-aware reward signals and multi-step reasoning for robust target identification.

D.4 RESULTS

We summarize detailed per-cohort results across various cancer types from TCGA in Figure 11 and Tables 8–35, demonstrating that GALAX achieves the highest performance across nearly all evaluated metrics and cancer cohorts. M2T, serving as a baseline relying solely on multi-omics data without any structured graph or language modeling, performs poorly, underscoring the necessity of incorporating richer contextual information. Adding graph structure via a pretrained Graph Attention Network (GAT) provides some improvements, albeit limited, indicating that static graph

representations alone are insufficient for capturing the complex biological interactions inherent in the data. To further elucidate the value of incorporating language models, we evaluate multiple LLaMA3 (L3) variants. Models that lack Target-specific finetuning, such as L3 combined only with omics data (L3) or with additional knowledge graphs (L3 + KG), deliver suboptimal performance, even with external knowledge enrichment. Biomedical-domain-specific finetuning (L3-FT(Med)) significantly enhances performance in identifying relevant targets, and integrating knowledge graphs yields modest incremental improvements. Nonetheless, even the variant supervised by Target-QA (L3-FT(QA) + KG) demonstrates limited additional benefit from knowledge graph integration, primarily due to its inability to dynamically generate structured subgraphs tailored to the reasoning task. The G-Retriever model, augmenting a pretrained graph attention network with retrieval mechanisms, achieves stronger performance compared to earlier baselines but remains limited by its absence of step-wise supervision and interpretability in biological reasoning. In contrast, GALAX uniquely integrates a Target-QA finetuned large language model, a pretrained Graph Attention Network, and a reinforcement learning-driven subgraph generator guided by a graph process reward model. This sophisticated architecture facilitates interpretable and biologically informed reasoning by dynamically generating structured subgraphs relevant to the biological context. Consequently, GALAX significantly surpasses all baseline models, achieving state-of-the-art performance across both overall average metrics and individual cancer cohort-specific evaluations.

E REINFORCEMENT LEARNING GENERATED SUBGRAPH DETAILS

Figure 12 provides a high-level overview of the explainable subgraphs of part of cell lines, highlighting key proteins and their predicted functional interactions that define the unique molecular signatures of each cell line. These interpretable network maps identify the most salient features prioritized by our model. To move beyond structural insights and assess their biological significance, we conduct enrichment analyses to evaluate whether the identified molecules are significantly over-represented in curated knowledge bases such as KEGG and WikiPathway. This analysis enables us to contextualize the salient features within relevant targets and signaling pathways. The resulting cell-line-specific interpretations bridge model-driven discovery with established biological knowledge and are detailed in the following sections.

Enrichment analysis of **sample ACH-000054 (HT-1080)**, representing fibrosarcoma (metastasis; SARC), revealed a significant association with **Sarcoma** (P-value = 1.625×10^{-4} , Adj.P = 4.08×10^{-2}) driven by **COL1A1**, **WWTR1**, **APAF1**, **PLK1**, **EPHB4**, and **SH2B1**. Pathway-level signals underscored apoptotic and stress-response programs, with strong enrichment of **Apoptosis Modulation by HSP70** (WP384; P-value = 1.864×10^{-6} , Adj.P = 1.45×10^{-4}) and **Apoptosis** (WP254; P-value = 1.73×10^{-4} , Adj.P = 5.26×10^{-3}), each supported by **MAPK10**, **APAF1**, and **TNFRSF1A**. Additional inflammatory and mitogenic axes were indicated by **TNF alpha Signaling Pathway** (WP231; P-value = 2.27×10^{-4} , Adj.P = 5.26×10^{-3}) involving **APAF1**, **PLK1**, and **TNFRSF1A**, and by the **MAPK Signaling Pathway** (WP382; P-value = 2.70×10^{-4} , Adj.P = 5.26×10^{-3}) featuring **MAPK10**, **DUSP1**, **RASGRF2**, and **TNFRSF1A**. Finally, **Nanoparticle-mediated activation of receptor signaling** (WP2643; P-value = 6.02×10^{-4} , Adj.P = 8.99×10^{-3}) highlighted extracellular matrix and receptor-proximal cues via **COL1A1** and **MAPK10**. Collectively, recurrent involvement of apoptosis regulators (**APAF1**, **TNFRSF1A**), MAPK components (**MAPK10**, **DUSP1**, **RASGRF2**), and proliferative drivers (**PLK1**) points to coordinated apoptotic, inflammatory, and receptor-MAPK signaling programs characteristic of fibrosarcoma biology.

For **sample ACH-000001 (NIH:OVCAR-3)**, an ovarian adenocarcinoma line (metastasis; OV), analysis indicated only a weak disease-level association with **ovarian cancer** (P-value = 1.41×10^{-1} , Adj.P = 1.65×10^{-1}), primarily linked to **ERBB2**. While this signal was not significant after multiple-testing correction, pathway-level evaluation revealed several strongly dysregulated processes. The **Prolactin Signaling Pathway** (WP2037; P-value = 2.90×10^{-4} , Adj.P = 1.49×10^{-2}) was prominently enriched through **RPS6KB1**, **NOS2**, and **ERBB2**, pointing to growth factor-driven oncogenic signaling. Similarly, enrichment of the **Leptin Signaling Pathway** (WP2034; P-value = 2.90×10^{-4} , Adj.P = 1.49×10^{-2}) and the **ErbB Signaling Pathway** (WP673; P-value = 4.92×10^{-4} , Adj.P = 1.69×10^{-2}) implicated **RPS6KB1**, **ERBB2**, and **PLCG2**, reflecting interconnected receptor tyrosine kinase and metabolic networks. Additional pathways included **IGF1-Akt signaling** (WP3850; P-value = 1.26×10^{-3} , Adj.P

Protein Signaling Networks Across Different Cancer Types

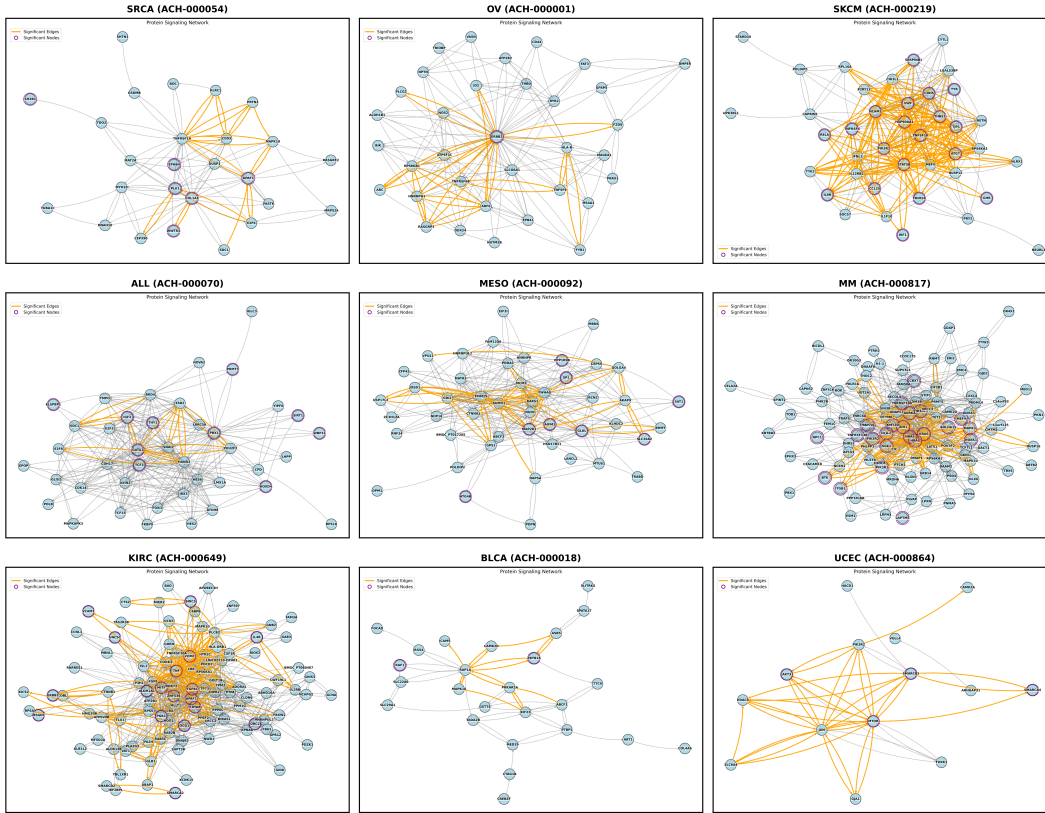


Figure 12: Part of explainable disease mechanism by core signaling subgraphs

= 3.09×10^{-2}) driven by **RPS6KB1** and **TNFSF9**, and **BDNF–TrkB Signaling** (WP3676; P-value = 1.52×10^{-3} , Adj.P = 3.09×10^{-2}) via **ARC** and **RPS6KB1**. These results underscore the central role of **ERBB2**-mediated receptor activity and downstream **RPS6KB1**-linked pathways, consistent with known mechanisms of ovarian carcinoma progression.

In **sample ACH-000219 (A-375)**, representing amelanotic melanoma (primary; SKCM), enrichment testing identified a highly significant signal for **melanoma** (P-value = 1.08×10^{-6} , Adj.P = 1.59×10^{-4}) supported by a broad gene panel including **CCL25**, **STAT5B**, **HSP90AA1**, **SERPINB1**, **VWF**, **TYR**, **THBS1**, **RELA**, **TJPI**, **GHR**, **CDH5**, **IRF1**, **TNFSF10**, **TRIM24**, **NCAM1**, **ATG7**, **TNFRSF4**, and **IL9R**. Immune and inflammatory cascades dominated the pathway enrichments, with the **NOD Pathway** (WP1433; P-value = 1.77×10^{-6} , Adj.P = 2.28×10^{-4}) enriched via **HSP90AA1**, **NLRP12**, **MEFV**, and **RELA**, pointing to innate immune activation. Cytokine-related processes were also evident, including the **IL-4 Signaling Pathway** (WP395; P-value = 5.42×10^{-6} , Adj.P = 2.65×10^{-4}) and the **IL-9 Signaling Pathway** (WP22; P-value = 6.16×10^{-6} , Adj.P = 2.65×10^{-4}), with contributions from **STAT5B**, **PIK3R1**, and **IL9R**, consistent with Th2/Th9 regulation. The **Oncostatin M Signaling Pathway** (WP2374; P-value = 1.14×10^{-5} , Adj.P = 3.60×10^{-4}) further implicated **STAT5B**, **TYK2**, **PIK3R1**, and **RELA**, linking cytokine–STAT and NF- κ B signaling to melanoma progression. Overall, repeated enrichment of **STAT5B**, **RELA**, and **PIK3R1** across pathways highlights coordinated dysregulation of inflammatory and cytokine signaling networks in amelanotic melanoma.

Enrichment analysis of **sample ACH-000070 (697)**, representing B-cell acute lymphoblastic leukemia (ALL) with the **t(1;19)(q23;p13.3) E2A–PBX1 (TCF3–PBX1)** translocation, revealed a strong disease-level association with **acute lymphocytic leukemia** (P-value = 7.37×10^{-5} , Adj.P = 8.10×10^{-3}) supported by genes including **IGF2**, **WBP1L**, **ELSPBP1**, **HOXD4**, **TCF3**, **THY1**, **SIRT1**, **GATA1**, and **PBX1**. Pathway enrichment further emphasized leukemia-relevant transcriptional programs: **Sudden Infant Death Syndrome (SIDS) Susceptibility Pathways** (WP706;

P-value = 3.02×10^{-4} , Adj.P = 1.94×10^{-2}) through **TCF3**, **POU2F2**, **ESR2**, and **PBX1**; and the **Wnt/ β -catenin Signaling Pathway in Leukemia** (WP3658; P-value = 1.29×10^{-3} , Adj.P = 4.13×10^{-2}) involving **AXIN2** and **TCF3**. Additional signals included the **Breast Cancer Pathway** (WP4262; P-value = 3.85×10^{-3} , Adj.P = 6.06×10^{-2}) with **E2F3**, **AXIN2**, and **ESR2**, and the broader **Wnt Signaling Pathway** (WP363; P-value = 5.10×10^{-3} , Adj.P = 6.06×10^{-2}) featuring **AXIN2** and **TCF3**. Collectively, these findings underscore recurrent involvement of the **TCF3–PBX1** fusion together with Wnt/ β -catenin signaling and leukemogenic transcription factors, consistent with the molecular etiology of this ALL subtype.

Enrichment analysis of **sample ACH-000092 (NCI-H2452)**, representing pleural mesothelioma (metastasis; MESO), showed a modest disease-level association with **Lung Neoplasms** (P-value = 4.965×10^{-3} , Adj.P = 1.89×10^{-1}) supported by **MAP2K1**, **SLC26A2**, **AIFM1**, **SP1**, **ATG4B**, **SAT1**, **GLUL**, and **PPP1R9B**. Pathway analysis highlighted metabolic and growth-factor–linked programs: **Amino Acid metabolism** (WP3925; P-value = 1.20×10^{-3} , Adj.P = 5.63×10^{-2}) involving **BHMT**, **PDHA1**, and **GLUL**; the **Estrogen signaling pathway** (WP712; P-value = 1.27×10^{-3} , Adj.P = 5.63×10^{-2}) marked by **MAP2K1** and **SP1**; and **TGF- β Signaling** (WP366; P-value = 3.47×10^{-3} , Adj.P = 1.15×10^{-1}) featuring **MAP2K1**, **SUMO1**, and **SP1**. Together, these results suggest coordinated amino acid metabolic rewiring and transcriptional control via MAPK–SP1 and TGF- β axes in the mesothelioma context.

Enrichment analysis of **sample ACH-000817 (RPMI 8226)**, representing plasma cell myeloma (primary; MM), revealed a highly significant association with **Multiple Myeloma** (P-value = 3.891×10^{-6} , Adj.P = 6.64×10^{-4}) supported by **ITGB1**, **KMT2D**, **CBX7**, **TNFRSF13B**, **IDH1**, **LAPTM5**, **HLA-C**, **TNFRSF10A**, **PIK3R2**, **KIR3DL1**, **BHLHA15**, **PIK3R1**, **MEFV**, **AURKA**, **NRAS**, **NUAK1**, **NPC1**, **BTK**, **KRAS**, **SGK1**, **HRAS**, **MAPK3**, and **FBXO9**. Pathway analysis further highlighted the **ErbB Signaling Pathway** (WP673; P-value = 8.47×10^{-8} , Adj.P = 1.03×10^{-5}) involving **MAPK10**, **CAMK2D**, **NRAS**, **PIK3R2**, **KRAS**, **PIK3R1**, **HRAS**, and **MAPK3**, indicating convergence of RAS–MAPK and PI3K effector cascades downstream of ErbB family receptors—features consistent with myeloma signaling dependencies and potential therapeutic vulnerabilities.

Enrichment analysis of **sample ACH-000649 (786-O)**, representing renal cell carcinoma (primary; KIRC), revealed a highly significant association with **Conventional (Clear Cell) Renal Cell Carcinoma** (P-value = 1.273×10^{-9} , Adj.P = 9.68×10^{-7}) supported by **TGFB1**, **IL4R**, **VCAM1**, **APAF1**, **OGG1**, **MSGN1**, **MITF**, **UNC5C**, **SMARCA2**, **TNF**, **POMC**, **FPGT**, **ORC2**, **ERBB2**, **ALDH1A1**, **PGK1**, **BIRC5**, **ZNF536**, **VHL**, and **CRYAB**. This gene set spans hallmark features of clear cell RCC biology, including hypoxia/VHL-axis signaling (**VHL**, **PGK1**), apoptosis regulation (**APAF1**, **BIRC5**), growth factor and RTK pathways (**ERBB2**, **TGFB1**), immune–inflammatory components (**TNF**, **IL4R**, **VCAM1**), metabolic and oxidative stress responses (**ALDH1A1**, **CRYAB**), and genome maintenance/chromatin remodeling (**OGG1**, **ORC2**, **SMARCA2**), collectively underscoring a prototypical clear cell transcriptomic signature.

Enrichment analysis of **sample ACH-000018 (T24)**, representing bladder carcinoma (primary; BLCA), showed a borderline disease-level signal for **Cancer** (P-value = 5.755×10^{-2} , Adj.P = 1.02×10^{-1}) driven by **ZBTB16** and **RAF1**. Pathway-level analysis revealed significant enrichment of **Focal Adhesion** (WP306; P-value = 1.17×10^{-4} , Adj.P = 1.03×10^{-2}) involving **MAPK10**, **RAP1A**, **COL4A6**, and **RAF1**; the **ErbB Signaling Pathway** (WP673; P-value = 2.20×10^{-4} , Adj.P = 1.03×10^{-2}) featuring **MAPK10**, **CAMK2D**, and **RAF1**; and **Integrin-mediated Cell Adhesion** (WP185; P-value = 2.99×10^{-4} , Adj.P = 1.03×10^{-2}) with **MAPK10**, **RAP1A**, and **RAF1**. Collectively, recurrent involvement of **RAF1** together with **MAPK10** across adhesion and ErbB-axis pathways points to convergent RTK–MAPK and integrin signaling programs in this BLCA context.

Enrichment analysis of **sample ACH-000864 (COLO 684)**, representing endometrial adenocarcinoma (primary; UCEC), revealed a highly significant disease-level association with **Carcinoma, Small Cell** (P-value = 1.064×10^{-6} , Adj.P = 1.29×10^{-4}) supported by **SMARCB1**, **AKT3**, **MTOR**, and **SMARCA4**. Pathway analysis highlighted potent receptor tyrosine kinase and stemness programs: the **ErbB Signaling Pathway** (WP673; P-value = 3.38×10^{-9} , Adj.P

= 4.90×10^{-7}) involving **JUN**, **CAMK2A**, **AKT3**, **PIK3R2**, and **MTOR**; the **EGF/EGFR Signaling Pathway** (WP437; P-value = 6.19×10^{-8} , Adj.P = 4.48×10^{-6}) through **JUN**, **GJA1**, **CAMK2A**, **PIK3R2**, and **MTOR**; and **ESC Pluripotency Pathways** (WP3931; P-value = 1.03×10^{-6} , Adj.P = 4.97×10^{-5}) marked by **JUN**, **AKT3**, **PIK3R2**, and **MTOR**. Collectively, recurrent involvement of **AKT3** and **MTOR**—together with **PIK3R2**, **JUN**, and **CAMK2A**—points to convergent EGFR/ErbB-PI3K-AKT-mTOR signaling and pluripotency-associated programs in this UCEC context.

Table 8: Model overall performances

Model	Precision \uparrow	Recall \uparrow	F1 \uparrow	Jaccard \uparrow	Hit@5 \uparrow	Hit@10 \uparrow
M2T	0.0016	0.0011	0.0013	0.0006	0.0000	0.0029
GAT	0.0006 \pm 0.0000	0.0006 \pm 0.0000	0.0006 \pm 0.0000	0.0003 \pm 0.0000	0.0000 \pm 0.0000	0.0000 \pm 0.0000
L3	0.0071 \pm 0.0032	0.0013 \pm 0.0002	0.0021 \pm 0.0002	0.0011 \pm 0.0001	0.0032 \pm 0.0055	0.0021 \pm 0.0037
L3 + KG	0.0125 \pm 0.0032	0.0029 \pm 0.0003	0.0043 \pm 0.0002	0.0022 \pm 0.0001	0.0085 \pm 0.0037	0.0122 \pm 0.0033
L3-FT(Med)	0.0179 \pm 0.0045	0.0133 \pm 0.0064	0.0115 \pm 0.0044	0.0059 \pm 0.0023	0.0116 \pm 0.0097	0.0122 \pm 0.0072
L3-FT(Med) + KG	0.0158 \pm 0.0030	0.0058 \pm 0.0011	0.0074 \pm 0.0016	0.0038 \pm 0.0010	0.0106 \pm 0.0048	0.0132 \pm 0.0040
L3-FT(QA)	0.5250 \pm 0.0282	0.4959 \pm 0.0435	0.5094 \pm 0.0365	0.3449 \pm 0.0338	0.8889 \pm 0.0168	0.8693 \pm 0.0157
L3-FT(QA) + KG	0.5185 \pm 0.0240	0.4908 \pm 0.0402	0.5038 \pm 0.0327	0.3393 \pm 0.0298	0.8794 \pm 0.0115	0.8529 \pm 0.0153
G-Retriever	0.4763 \pm 0.0004	0.3929 \pm 0.0063	0.4286 \pm 0.0044	0.2757 \pm 0.0038	0.8804 \pm 0.0037	0.8550 \pm 0.0046
GALAX	0.5472\pm0.0053	0.5332\pm0.0031	0.5399\pm0.0041	0.3726\pm0.0037	0.9249\pm0.0048	0.8815\pm0.0033

Table 9: Model performances on LUAD

Model	Precision \uparrow	Recall \uparrow	F1 \uparrow	Jaccard \uparrow	Hit@5 \uparrow	Hit@10 \uparrow
M2T	0.0020	0.0014	0.0017	0.0008	0.0000	0.0000
GAT	0.0000 \pm 0.0000					
L3	0.0079 \pm 0.0137	0.0005 \pm 0.0008	0.0009 \pm 0.0016	0.0005 \pm 0.0008	0.0095 \pm 0.0165	0.0048 \pm 0.0082
L3 + KG	0.0014 \pm 0.0025	0.0010 \pm 0.0017	0.0011 \pm 0.0020	0.0006 \pm 0.0010	0.0000 \pm 0.0000	0.0000 \pm 0.0000
L3-FT(Med)	0.0091 \pm 0.0018	0.0105 \pm 0.0044	0.0079 \pm 0.0022	0.0040 \pm 0.0011	0.0000 \pm 0.0000	0.0000 \pm 0.0000
L3-FT(Med) + KG	0.0081 \pm 0.0071	0.0024 \pm 0.0017	0.0025 \pm 0.0002	0.0013 \pm 0.0001	0.0095 \pm 0.0165	0.0048 \pm 0.0082
L3-FT(QA)	0.5201 \pm 0.0408	0.4905 \pm 0.0532	0.5045 \pm 0.0475	0.3396 \pm 0.0433	0.8476 \pm 0.0165	0.8667 \pm 0.0218
L3-FT(QA) + KG	0.5214 \pm 0.0242	0.4952 \pm 0.0432	0.5073 \pm 0.0343	0.3416 \pm 0.0314	0.7905 \pm 0.0436	0.8048 \pm 0.0541
G-Retriever	0.4642 \pm 0.0181	0.3881 \pm 0.0264	0.4204 \pm 0.0233	0.2671 \pm 0.0188	0.8857 \pm 0.0000	0.8524 \pm 0.0165
GALAX	0.5345\pm0.0185	0.5157\pm0.0043	0.5247\pm0.0109	0.3581\pm0.0101	0.9238\pm0.0436	0.8810\pm0.0082

Table 10: Model performances on BRCA

Model	Precision \uparrow	Recall \uparrow	F1 \uparrow	Jaccard \uparrow	Hit@5 \uparrow	Hit@10 \uparrow
M2T	0.0000	0.0000	0.0000	0.0000	0.0000	0.0000
GAT	0.0033 \pm 0.0000	0.0033 \pm 0.0000	0.0033 \pm 0.0000	0.0017 \pm 0.0000	0.0000 \pm 0.0000	0.0000 \pm 0.0000
L3	0.0020 \pm 0.0035	0.0017 \pm 0.0029	0.0018 \pm 0.0032	0.0009 \pm 0.0016	0.0000 \pm 0.0000	0.0000 \pm 0.0000
L3 + KG	0.0073 \pm 0.0068	0.0033 \pm 0.0029	0.0044 \pm 0.0038	0.0022 \pm 0.0019	0.0111 \pm 0.0192	0.0056 \pm 0.0096
L3-FT(Med)	0.0110 \pm 0.0086	0.0106 \pm 0.0075	0.0093 \pm 0.0068	0.0047 \pm 0.0035	0.0000 \pm 0.0000	0.0111 \pm 0.0192
L3-FT(Med) + KG	0.0149 \pm 0.0057	0.0050 \pm 0.0000	0.0071 \pm 0.0012	0.0036 \pm 0.0006	0.0000 \pm 0.0000	0.0111 \pm 0.0192
L3-FT(QA)	0.5074 \pm 0.0498	0.4856 \pm 0.0570	0.4956 \pm 0.0535	0.3336 \pm 0.0491	0.8889\pm0.0509	0.8389 \pm 0.0096
L3-FT(QA) + KG	0.4856 \pm 0.0395	0.4656 \pm 0.0436	0.4751 \pm 0.0412	0.3142 \pm 0.0354	0.8778 \pm 0.0192	0.8222 \pm 0.0347
G-Retriever	0.4414 \pm 0.0099	0.3772 \pm 0.0010	0.4062 \pm 0.0034	0.2607 \pm 0.0032	0.8667 \pm 0.0000	0.8667\pm0.0000
GALAX	0.5608\pm0.0031	0.5533\pm0.0033	0.5569\pm0.0028	0.3886\pm0.0022	0.8889\pm0.0839	0.8500 \pm 0.0441

Table 11: Model performances on COAD/READ

Model	Precision \uparrow	Recall \uparrow	F1 \uparrow	Jaccard \uparrow	Hit@5 \uparrow	Hit@10 \uparrow
M2T	0.0023	0.0017	0.0019	0.0010	0.0000	0.0000
GAT	0.0000 \pm 0.0000					
L3	0.0233 \pm 0.0252	0.0020 \pm 0.0020	0.0035 \pm 0.0033	0.0018 \pm 0.0017	0.0133 \pm 0.0231	0.0067 \pm 0.0115
L3 + KG	0.0055 \pm 0.0055	0.0033 \pm 0.0031	0.0041 \pm 0.0039	0.0021 \pm 0.0020	0.0000 \pm 0.0000	0.0000 \pm 0.0000
L3-FT(Med)	0.0300 \pm 0.0249	0.0220 \pm 0.0278	0.0199 \pm 0.0214	0.0104 \pm 0.0114	0.0267 \pm 0.0462	0.0333 \pm 0.0306
L3-FT(Med) + KG	0.0044 \pm 0.0038	0.0033 \pm 0.0031	0.0032 \pm 0.0028	0.0016 \pm 0.0014	0.0000 \pm 0.0000	0.0000 \pm 0.0000
L3-FT(QA)	0.5011 \pm 0.0335	0.4727 \pm 0.0514	0.4862 \pm 0.0430	0.3230 \pm 0.0384	0.8400 \pm 0.0800	0.8267 \pm 0.0808
L3-FT(QA) + KG	0.5116 \pm 0.0216	0.4807 \pm 0.0469	0.4950 \pm 0.0351	0.3301 \pm 0.0312	0.8800 \pm 0.0000	0.8333 \pm 0.0231
G-Retriever	0.4417 \pm 0.0005	0.3680 \pm 0.0104	0.3995 \pm 0.0073	0.2504 \pm 0.0062	0.7200 \pm 0.0000	0.7667 \pm 0.0115
GALAX	0.5272\pm0.0143	0.5120\pm0.0087	0.5192\pm0.0103	0.3512\pm0.0098	0.9200\pm0.0693	0.8400\pm0.0200

Table 12: Model performances on PAAD

Model	Precision \uparrow	Recall \uparrow	F1 \uparrow	Jaccard \uparrow	Hit@5 \uparrow	Hit@10 \uparrow
M2T	0.0017	0.0013	0.0014	0.0008	0.0000	0.0000
GAT	0.0025 \pm 0.0000	0.0025 \pm 0.0000	0.0025 \pm 0.0000	0.0013 \pm 0.0000	0.0000 \pm 0.0000	0.0000 \pm 0.0000
L3	0.0000 \pm 0.0000					
L3 + KG	0.0139 \pm 0.0241	0.0008 \pm 0.0014	0.0016 \pm 0.0027	0.0008 \pm 0.0014	0.0167 \pm 0.0289	0.0083 \pm 0.0144
L3-FT(Med)	0.0051 \pm 0.0061	0.0050 \pm 0.0043	0.0039 \pm 0.0036	0.0020 \pm 0.0018	0.0167 \pm 0.0289	0.0083 \pm 0.0144
L3-FT(Med) + KG	0.0005 \pm 0.0008	0.0008 \pm 0.0014	0.0006 \pm 0.0010	0.0003 \pm 0.0005	0.0000 \pm 0.0000	0.0000 \pm 0.0000
L3-FT(QA)	0.5649 \pm 0.0559	0.5358 \pm 0.0686	0.5492 \pm 0.0605	0.3811 \pm 0.0584	0.8000 \pm 0.0500	0.8417 \pm 0.0577
L3-FT(QA) + KG	0.5499 \pm 0.0570	0.5183 \pm 0.0794	0.5330 \pm 0.0683	0.3657 \pm 0.0650	0.8333 \pm 0.0764	0.8333 \pm 0.0520
G-Retriever	0.5594 \pm 0.0114	0.4567 \pm 0.0058	0.5016 \pm 0.0009	0.3387 \pm 0.0007	0.8500 \pm 0.0000	0.8500 \pm 0.0000
GALAX	0.5771 \pm 0.0174	0.5708 \pm 0.0118	0.5739 \pm 0.0145	0.4044 \pm 0.0154	0.8333 \pm 0.0289	0.8500 \pm 0.0000

Table 13: Model performances on GBM

Model	Precision \uparrow	Recall \uparrow	F1 \uparrow	Jaccard \uparrow	Hit@5 \uparrow	Hit@10 \uparrow
M2T	0.0000	0.0000	0.0000	0.0000	0.0000	0.0000
GAT	0.0000 \pm 0.0000					
L3	0.0056 \pm 0.0096	0.0011 \pm 0.0019	0.0019 \pm 0.0032	0.0009 \pm 0.0016	0.0000 \pm 0.0000	0.0000 \pm 0.0000
L3 + KG	0.0000 \pm 0.0000					
L3-FT(Med)	0.0069 \pm 0.0045	0.0133 \pm 0.0088	0.0090 \pm 0.0059	0.0046 \pm 0.0030	0.0000 \pm 0.0000	0.0000 \pm 0.0000
L3-FT(Med) + KG	0.0107 \pm 0.0158	0.0056 \pm 0.0038	0.0064 \pm 0.0074	0.0032 \pm 0.0037	0.0000 \pm 0.0000	0.0000 \pm 0.0000
L3-FT(QA)	0.5641 \pm 0.0310	0.5333 \pm 0.0462	0.5480 \pm 0.0387	0.3794 \pm 0.0364	0.9333 \pm 0.0667	0.9000 \pm 0.0333
L3-FT(QA) + KG	0.5391 \pm 0.0213	0.5178 \pm 0.0164	0.5281 \pm 0.0181	0.3596 \pm 0.0165	0.9556 \pm 0.0385	0.8444 \pm 0.0694
G-Retriever	0.4906 \pm 0.0075	0.4411 \pm 0.0038	0.4642 \pm 0.0010	0.3037 \pm 0.0000	0.9556 \pm 0.0385	0.8333 \pm 0.0577
GALAX	0.5527 \pm 0.0021	0.5422 \pm 0.0139	0.5473 \pm 0.0082	0.3769 \pm 0.0079	0.9111 \pm 0.0770	0.8667 \pm 0.0000

Table 14: Model performances on SARC

Model	Precision \uparrow	Recall \uparrow	F1 \uparrow	Jaccard \uparrow	Hit@5 \uparrow	Hit@10 \uparrow
M2T	0.0047	0.0033	0.0039	0.0019	0.0000	0.0000
GAT	0.0000 \pm 0.0000					
L3	0.0111 \pm 0.0192	0.0033 \pm 0.0058	0.0051 \pm 0.0089	0.0026 \pm 0.0045	0.0000 \pm 0.0000	0.0000 \pm 0.0000
L3 + KG	0.0271 \pm 0.0062	0.0111 \pm 0.0019	0.0157 \pm 0.0029	0.0080 \pm 0.0015	0.0222 \pm 0.0385	0.0222 \pm 0.0192
L3-FT(Med)	0.0689 \pm 0.0631	0.0167 \pm 0.0115	0.0229 \pm 0.0180	0.0119 \pm 0.0094	0.0222 \pm 0.0385	0.0667 \pm 0.0577
L3-FT(Med) + KG	0.0270 \pm 0.0108	0.0089 \pm 0.0019	0.0120 \pm 0.0009	0.0061 \pm 0.0005	0.0222 \pm 0.0385	0.0222 \pm 0.0192
L3-FT(QA)	0.5347 \pm 0.0167	0.5089 \pm 0.0353	0.5211 \pm 0.0266	0.3547 \pm 0.0253	0.9111 \pm 0.0385	0.8778 \pm 0.0192
L3-FT(QA) + KG	0.5423 \pm 0.0207	0.5022 \pm 0.0539	0.5207 \pm 0.0383	0.3570 \pm 0.0344	0.8444 \pm 0.0385	0.8444 \pm 0.0385
G-Retriever	0.4461 \pm 0.0308	0.3667 \pm 0.0115	0.4009 \pm 0.0055	0.2518 \pm 0.0051	0.8667 \pm 0.0000	0.9222 \pm 0.0192
GALAX	0.5414 \pm 0.0143	0.5144 \pm 0.0168	0.5271 \pm 0.0157	0.3602 \pm 0.0165	0.9111 \pm 0.0108	0.8444 \pm 0.0509

Table 15: Model performances on OV

Model	Precision \uparrow	Recall \uparrow	F1 \uparrow	Jaccard \uparrow	Hit@5 \uparrow	Hit@10 \uparrow
M2T	0.0000	0.0000	0.0000	0.0000	0.0000	0.0000
GAT	0.0000 \pm 0.0000					
L3	0.0241 \pm 0.0251	0.0044 \pm 0.0051	0.0075 \pm 0.0085	0.0038 \pm 0.0043	0.0000 \pm 0.0000	0.0111 \pm 0.0192
L3 + KG	0.0660 \pm 0.0667	0.0111 \pm 0.0102	0.0183 \pm 0.0161	0.0093 \pm 0.0082	0.0000 \pm 0.0000	0.0889 \pm 0.0770
L3-FT(Med)	0.0356 \pm 0.0412	0.0100 \pm 0.0067	0.0102 \pm 0.0072	0.0051 \pm 0.0036	0.0444 \pm 0.0770	0.0222 \pm 0.0385
L3-FT(Med) + KG	0.0797 \pm 0.0496	0.0344 \pm 0.0280	0.0457 \pm 0.0375	0.0253 \pm 0.0226	0.0000 \pm 0.0000	0.0333 \pm 0.0333
L3-FT(QA)	0.5469 \pm 0.0274	0.5167 \pm 0.0406	0.5307 \pm 0.0325	0.3631 \pm 0.0295	1.0000 \pm 0.0000	0.9111 \pm 0.0694
L3-FT(QA) + KG	0.5439 \pm 0.0066	0.4989 \pm 0.0195	0.5200 \pm 0.0123	0.3542 \pm 0.0095	0.9556 \pm 0.0385	0.9444 \pm 0.0385
G-Retriever	0.5413 \pm 0.0525	0.4033 \pm 0.0173	0.4575 \pm 0.0067	0.2991 \pm 0.0041	1.0000 \pm 0.0000	0.9667 \pm 0.0000
GALAX	0.5489 \pm 0.0176	0.5344 \pm 0.0259	0.5413 \pm 0.0219	0.3714 \pm 0.0206	0.8444 \pm 0.0385	0.8667 \pm 0.0333

Table 16: Model performances on SKCM

Model	Precision \uparrow	Recall \uparrow	F1 \uparrow	Jaccard \uparrow	Hit@5 \uparrow	Hit@10 \uparrow
M2T	0.0055	0.0033	0.0041	0.0021	0.0000	0.0333
GAT	0.0000 \pm 0.0000					
L3	0.0000 \pm 0.0000					
L3 + KG	0.0028 \pm 0.0049	0.0011 \pm 0.0019	0.0016 \pm 0.0028	0.0008 \pm 0.0014	0.0000 \pm 0.0000	0.0111 \pm 0.0192
L3-FT(Med)	0.0047 \pm 0.0041	0.0089 \pm 0.0069	0.0061 \pm 0.0052	0.0031 \pm 0.0026	0.0000 \pm 0.0000	0.0000 \pm 0.0000
L3-FT(Med) + KG	0.0000 \pm 0.0000					
L3-FT(QA)	0.5145 \pm 0.0437	0.4922 \pm 0.0455	0.5028 \pm 0.0443	0.3399 \pm 0.0401	0.8444 \pm 0.1388	0.8556 \pm 0.0385
L3-FT(QA) + KG	0.4871 \pm 0.0529	0.4678 \pm 0.0626	0.4771 \pm 0.0579	0.3164 \pm 0.0514	0.8667 \pm 0.0667	0.8667 \pm 0.0667
G-Retriever	0.5123 \pm 0.0545	0.4100 \pm 0.0058	0.4543 \pm 0.0258	0.2958 \pm 0.0222	0.9333 \pm 0.0000	0.8778 \pm 0.0192
GALAX	0.5385 \pm 0.0116	0.5233 \pm 0.0200	0.5307 \pm 0.0160	0.3638 \pm 0.0152	1.0000 \pm 0.0000	0.9667 \pm 0.0000

Table 17: Model performances on ESCA

Model	Precision \uparrow	Recall \uparrow	F1 \uparrow	Jaccard \uparrow	Hit@5 \uparrow	Hit@10 \uparrow
M2T	0.0000	0.0000	0.0000	0.0000	0.0000	0.0000
GAT	0.0000 \pm 0.0000					
L3	0.0000 \pm 0.0000					
L3 + KG	0.0028 \pm 0.0049	0.0011 \pm 0.0019	0.0016 \pm 0.0028	0.0008 \pm 0.0014	0.0000 \pm 0.0000	0.0111 \pm 0.0192
L3-FT(Med)	0.0047 \pm 0.0041	0.0089 \pm 0.0069	0.0061 \pm 0.0052	0.0031 \pm 0.0026	0.0000 \pm 0.0000	0.0000 \pm 0.0000
L3-FT(Med) + KG	0.0000 \pm 0.0000					
L3-FT(QA)	0.5210 \pm 0.0590	0.4989 \pm 0.0691	0.5093 \pm 0.0637	0.3438 \pm 0.0577	0.9333 \pm 0.0667	0.9333 \pm 0.0000
L3-FT(QA) + KG	0.5146 \pm 0.0187	0.4878 \pm 0.0051	0.5003 \pm 0.0074	0.3346 \pm 0.0059	0.9111 \pm 0.0385	0.9333 \pm 0.0000
G-Retriever	0.5083 \pm 0.0142	0.4156 \pm 0.0038	0.4556 \pm 0.0076	0.2959 \pm 0.0064	0.9778\pm0.0385	0.9444 \pm 0.0385
GALAX	0.5775\pm0.0204	0.5667\pm0.0260	0.5720\pm0.0233	0.4031\pm0.0246	0.9556 \pm 0.0385	0.9667\pm0.0333

Table 18: Model performances on SCLC

Model	Precision \uparrow	Recall \uparrow	F1 \uparrow	Jaccard \uparrow	Hit@5 \uparrow	Hit@10 \uparrow
M2T	0.0000	0.0000	0.0000	0.0000	0.0000	0.0000
GAT	0.0000 \pm 0.0000					
L3	0.0000 \pm 0.0000					
L3 + KG	0.0000 \pm 0.0000					
L3-FT(Med)	0.0184 \pm 0.0212	0.0389 \pm 0.0448	0.0249 \pm 0.0286	0.0131 \pm 0.0153	0.0000 \pm 0.0000	0.0000 \pm 0.0000
L3-FT(Med) + KG	0.0000 \pm 0.0000					
L3-FT(QA)	0.5337 \pm 0.0349	0.4989 \pm 0.0479	0.5146 \pm 0.0378	0.3476 \pm 0.0341	0.8667 \pm 0.1155	0.8556 \pm 0.0694
L3-FT(QA) + KG	0.4900 \pm 0.0597	0.4667 \pm 0.0677	0.4778 \pm 0.0638	0.3160 \pm 0.0555	0.9333 \pm 0.0667	0.8778 \pm 0.0694
G-Retriever	0.4203 \pm 0.0263	0.3667 \pm 0.0115	0.3910 \pm 0.0180	0.2434 \pm 0.0140	0.8667 \pm 0.0000	0.8000 \pm 0.0000
GALAX	0.5850\pm0.0110	0.5822\pm0.0102	0.5836\pm0.0105	0.4143\pm0.0102	0.9778\pm0.0385	0.9000\pm0.0333

Table 19: Model performances on HNSC

Model	Precision \uparrow	Recall \uparrow	F1 \uparrow	Jaccard \uparrow	Hit@5 \uparrow	Hit@10 \uparrow
M2T	0.0000	0.0000	0.0000	0.0000	0.0000	0.0000
GAT	0.0000 \pm 0.0000					
L3	0.0000 \pm 0.0000					
L3 + KG	0.0128 \pm 0.0222	0.0017 \pm 0.0029	0.0030 \pm 0.0051	0.0015 \pm 0.0026	0.0333 \pm 0.0577	0.0167 \pm 0.0289
L3-FT(Med)	0.0082 \pm 0.0036	0.0100 \pm 0.0050	0.0079 \pm 0.0016	0.0040 \pm 0.0008	0.0000 \pm 0.0000	0.0000 \pm 0.0000
L3-FT(Med) + KG	0.0000 \pm 0.0000					
L3-FT(QA)	0.4374 \pm 0.0214	0.4167 \pm 0.0208	0.4267 \pm 0.0208	0.2718 \pm 0.0174	1.0000\pm0.0000	0.9667\pm0.0577
L3-FT(QA) + KG	0.4787\pm0.0445	0.4450\pm0.0676	0.4606\pm0.0565	0.3006\pm0.0470	0.9667 \pm 0.0577	0.9500 \pm 0.0000
G-Retriever	0.4413 \pm 0.0030	0.3700 \pm 0.0000	0.4021 \pm 0.0009	0.2518 \pm 0.0008	1.0000\pm0.0000	0.9500 \pm 0.0000
GALAX	0.4482 \pm 0.0229	0.4283 \pm 0.0208	0.4380 \pm 0.0218	0.2822 \pm 0.0177	0.9333 \pm 0.0577	0.9667\pm0.0289

Table 20: Model performances on LUSC

Model	Precision \uparrow	Recall \uparrow	F1 \uparrow	Jaccard \uparrow	Hit@5 \uparrow	Hit@10 \uparrow
M2T	0.0000	0.0000	0.0000	0.0000	0.0000	0.0000
GAT	0.0000 \pm 0.0000					
L3	0.0222 \pm 0.0192	0.0067 \pm 0.0058	0.0103 \pm 0.0089	0.0052 \pm 0.0045	0.0000 \pm 0.0000	0.0000 \pm 0.0000
L3 + KG	0.0062 \pm 0.0068	0.0050 \pm 0.0050	0.0055 \pm 0.0058	0.0028 \pm 0.0029	0.0000 \pm 0.0000	0.0000 \pm 0.0000
L3-FT(Med)	0.0165 \pm 0.0106	0.0083 \pm 0.0058	0.0085 \pm 0.0010	0.0043 \pm 0.0005	0.0000 \pm 0.0000	0.0000 \pm 0.0000
L3-FT(Med) + KG	0.0094 \pm 0.0082	0.0033 \pm 0.0029	0.0049 \pm 0.0043	0.0025 \pm 0.0021	0.0000 \pm 0.0000	0.0000 \pm 0.0000
L3-FT(QA)	0.5208\pm0.0525	0.4767 \pm 0.0810	0.4961\pm0.0677	0.3320\pm0.0618	0.9667 \pm 0.0577	0.9167 \pm 0.0577
L3-FT(QA) + KG	0.4656 \pm 0.0253	0.4217 \pm 0.0584	0.4420 \pm 0.0427	0.2844 \pm 0.0355	0.9333 \pm 0.1155	0.9333\pm0.0577
G-Retriever	0.4563 \pm 0.0579	0.3417 \pm 0.0318	0.3902 \pm 0.0418	0.2433 \pm 0.0313	1.0000\pm0.0000	0.9000 \pm 0.0000
GALAX	0.5046 \pm 0.0833	0.4783\pm0.0808	0.4909 \pm 0.0819	0.3285 \pm 0.0726	1.0000\pm0.0000	0.8833 \pm 0.0289

Table 21: Model performances on STAD

Model	Precision \uparrow	Recall \uparrow	F1 \uparrow	Jaccard \uparrow	Hit@5 \uparrow	Hit@10 \uparrow
M2T	0.0000	0.0000	0.0000	0.0000	0.0000	0.0000
GAT	0.0000 \pm 0.0000					
L3	0.0000 \pm 0.0000					
L3 + KG	0.0000 \pm 0.0000					
L3-FT(Med)	0.0057 \pm 0.0100	0.0017 \pm 0.0029	0.0026 \pm 0.0045	0.0013 \pm 0.0023	0.0000 \pm 0.0000	0.0167 \pm 0.0289
L3-FT(Med) + KG	0.0000 \pm 0.0000					
L3-FT(QA)	0.5528 \pm 0.0311	0.5200\pm0.0409	0.5353\pm0.0325	0.3684\pm0.0309	0.9333 \pm 0.0577	0.9333\pm0.0289
L3-FT(QA) + KG	0.5305 \pm 0.0231	0.5000 \pm 0.0427	0.5144 \pm 0.0332	0.3486 \pm 0.0322	0.9000 \pm 0.0000	0.8667 \pm 0.0289
G-Retriever	0.5574\pm0.0091	0.4883 \pm 0.0029	0.5193 \pm 0.0024	0.3550 \pm 0.0043	0.9000 \pm 0.0000	0.9000 \pm 0.0000
GALAX	0.5298 \pm 0.0331	0.4983 \pm 0.0404	0.5134 \pm 0.0371	0.3465 \pm 0.0338	0.9667\pm0.0577	0.8667 \pm 0.0289

Table 22: Model performances on MB

Model	Precision \uparrow	Recall \uparrow	F1 \uparrow	Jaccard \uparrow	Hit@5 \uparrow	Hit@10 \uparrow
M2T	0.0000	0.0000	0.0000	0.0000	0.0000	0.0000
GAT	0.0000 \pm 0.0000					
L3	0.0333 \pm 0.0577	0.0067 \pm 0.0115	0.0111 \pm 0.0192	0.0057 \pm 0.0098	0.0000 \pm 0.0000	0.0000 \pm 0.0000
L3 + KG	0.0126 \pm 0.0218	0.0067 \pm 0.0115	0.0087 \pm 0.0151	0.0044 \pm 0.0076	0.0000 \pm 0.0000	0.0000 \pm 0.0000
L3-FT(Med)	0.0177 \pm 0.0215	0.0100 \pm 0.0100	0.0102 \pm 0.0089	0.0052 \pm 0.0045	0.0000 \pm 0.0000	0.0000 \pm 0.0000
L3-FT(Med) + KG	0.0282 \pm 0.0237	0.0167 \pm 0.0058	0.0192 \pm 0.0090	0.0097 \pm 0.0046	0.0667 \pm 0.1155	0.0333 \pm 0.0577
L3-FT(QA)	0.5308 \pm 0.0327	0.5033\pm0.0551	0.5164\pm0.0440	0.3489\pm0.0394	0.8667 \pm 0.1155	0.8000 \pm 0.1000
L3-FT(QA) + KG	0.5086 \pm 0.0633	0.5000 \pm 0.0608	0.5043 \pm 0.0620	0.3387 \pm 0.0569	0.7333 \pm 0.2309	0.7000 \pm 0.2000
G-Retriever	0.5546\pm0.0421	0.3600 \pm 0.0173	0.4365 \pm 0.0257	0.2795 \pm 0.0213	0.8000 \pm 0.0000	0.7000 \pm 0.0000
GALAX	0.4897 \pm 0.0304	0.4867 \pm 0.0351	0.4882 \pm 0.0328	0.3233 \pm 0.0286	1.0000\pm0.0000	0.8333\pm0.0577

Table 23: Model performances on ALL

Model	Precision \uparrow	Recall \uparrow	F1 \uparrow	Jaccard \uparrow	Hit@5 \uparrow	Hit@10 \uparrow
M2T	0.0082	0.0050	0.0062	0.0031	0.0000	0.0500
GAT	0.0000 \pm 0.0000					
L3	0.0333 \pm 0.0577	0.0033 \pm 0.0058	0.0061 \pm 0.0105	0.0031 \pm 0.0053	0.0667 \pm 0.1155	0.0333 \pm 0.0577
L3 + KG	0.0000 \pm 0.0000					
L3-FT(Med)	0.0015 \pm 0.0026	0.0033 \pm 0.0058	0.0021 \pm 0.0036	0.0010 \pm 0.0018	0.0000 \pm 0.0000	0.0000 \pm 0.0000
L3-FT(Med) + KG	0.0607 \pm 0.0528	0.0133 \pm 0.0115	0.0219 \pm 0.0189	0.0111 \pm 0.0096	0.0000 \pm 0.0000	0.0000 \pm 0.0000
L3-FT(QA)	0.5487 \pm 0.0561	0.5400 \pm 0.0625	0.5443 \pm 0.0592	0.3754 \pm 0.0569	1.0000\pm0.0000	0.9333\pm0.1155
L3-FT(QA) + KG	0.6010 \pm 0.0608	0.5600 \pm 0.1100	0.5786 \pm 0.0868	0.4106 \pm 0.0872	0.9333 \pm 0.1155	0.9333\pm0.1155
G-Retriever	0.6285 \pm 0.0043	0.5300 \pm 0.0000	0.5750 \pm 0.0018	0.4036 \pm 0.0018	0.8000 \pm 0.0000	0.8000 \pm 0.0000
GALAX	0.6860\pm0.0246	0.6700\pm0.0265	0.6779\pm0.0255	0.5131\pm0.0295	1.0000\pm0.0000	0.9333\pm0.0577

Table 24: Model performances on LGG

Model	Precision \uparrow	Recall \uparrow	F1 \uparrow	Jaccard \uparrow	Hit@5 \uparrow	Hit@10 \uparrow
M2T	0.0000	0.0000	0.0000	0.0000	0.0000	0.0000
GAT	0.0000 \pm 0.0000					
L3	0.0000 \pm 0.0000					
L3 + KG	0.0053 \pm 0.0092	0.0033 \pm 0.0058	0.0041 \pm 0.0071	0.0021 \pm 0.0036	0.0000 \pm 0.0000	0.0000 \pm 0.0000
L3-FT(Med)	0.0070 \pm 0.0121	0.0133 \pm 0.0231	0.0092 \pm 0.0159	0.0046 \pm 0.0080	0.0000 \pm 0.0000	0.0000 \pm 0.0000
L3-FT(Med) + KG	0.0000 \pm 0.0000					
L3-FT(QA)	0.5000 \pm 0.0500	0.4367 \pm 0.0702	0.4649 \pm 0.0545	0.3040 \pm 0.0457	1.0000\pm0.0000	0.9667\pm0.0577
L3-FT(QA) + KG	0.5267 \pm 0.0250	0.5067 \pm 0.0115	0.5163 \pm 0.0141	0.3480 \pm 0.0128	1.0000\pm0.0000	0.9000 \pm 0.1000
G-Retriever	0.4846 \pm 0.0537	0.4300 \pm 0.0173	0.4540 \pm 0.0126	0.2937 \pm 0.0106	1.0000\pm0.0000	0.9000 \pm 0.0000
GALAX	0.5433\pm0.0252	0.5433\pm0.0252	0.5433\pm0.0252	0.3733\pm0.0238	1.0000\pm0.0000	0.9000 \pm 0.0000

Table 25: Model performances on NB

Model	Precision \uparrow	Recall \uparrow	F1 \uparrow	Jaccard \uparrow	Hit@5 \uparrow	Hit@10 \uparrow
M2T	0.0000	0.0000	0.0000	0.0000	0.0000	0.0000
GAT	0.0000 \pm 0.0000					
L3	0.0000 \pm 0.0000					
L3 + KG	0.0000 \pm 0.0000					
L3-FT(Med)	0.0085 \pm 0.0148	0.0167 \pm 0.0289	0.0113 \pm 0.0196	0.0057 \pm 0.0100	0.0000 \pm 0.0000	0.0000 \pm 0.0000
L3-FT(Med) + KG	0.0000 \pm 0.0000					
L3-FT(QA)	0.5597\pm0.0479	0.5233 \pm 0.0651	0.5407 \pm 0.0559	0.3718 \pm 0.0523	0.8667 \pm 0.2309	0.8667 \pm 0.1528
L3-FT(QA) + KG	0.5507 \pm 0.0704	0.5067 \pm 0.0723	0.5275 \pm 0.0703	0.3603 \pm 0.0667	0.9333 \pm 0.1155	0.8667 \pm 0.0577
G-Retriever	0.4322 \pm 0.0444	0.3933 \pm 0.0404	0.4119 \pm 0.0423	0.2599 \pm 0.0341	1.0000\pm0.0000	0.9333\pm0.0577
GALAX	0.5533 \pm 0.0115	0.5533\pm0.0115	0.5533\pm0.0115	0.3825\pm0.0110	0.8667 \pm 0.1155	0.8667 \pm 0.0577

Table 26: Model performances on MESO

Model	Precision \uparrow	Recall \uparrow	F1 \uparrow	Jaccard \uparrow	Hit@5 \uparrow	Hit@10 \uparrow
M2T	0.0070	0.0050	0.0058	0.0029	0.0000	0.0000
GAT	0.0000 \pm 0.0000					
L3	0.0000 \pm 0.0000					
L3 + KG	0.0000 \pm 0.0000					
L3-FT(Med)	0.0190 \pm 0.0201	0.0167 \pm 0.0208	0.0133 \pm 0.0121	0.0067 \pm 0.0061	0.0000 \pm 0.0000	0.0000 \pm 0.0000
L3-FT(Med) + KG	0.0192 \pm 0.0228	0.0100 \pm 0.0000	0.0104 \pm 0.0052	0.0053 \pm 0.0026	0.0000 \pm 0.0000	0.0000 \pm 0.0000
L3-FT(QA)	0.5182 \pm 0.0806	0.4833 \pm 0.0874	0.4995 \pm 0.0808	0.3354 \pm 0.0720	0.9333 \pm 0.1155	0.8667 \pm 0.1528
L3-FT(QA) + KG	0.5417 \pm 0.0419	0.5233 \pm 0.0416	0.5322 \pm 0.0402	0.3633 \pm 0.0374	0.8667 \pm 0.1155	0.9000\pm0.0000
G-Retriever	0.4721 \pm 0.0072	0.3733 \pm 0.0462	0.4161 \pm 0.0324	0.2630 \pm 0.0255	1.0000\pm0.0000	0.8000 \pm 0.0000
GALAX	0.5933\pm0.0231	0.5933\pm0.0231	0.5933\pm0.0231	0.4221\pm0.0236	1.0000\pm0.0000	0.8000 \pm 0.0000

Table 27: Model performances on LIHC

Model	Precision \uparrow	Recall \uparrow	F1 \uparrow	Jaccard \uparrow	Hit@5 \uparrow	Hit@10 \uparrow
M2T	0.0000	0.0000	0.0000	0.0000	0.0000	0.0000
GAT	0.0100 \pm 0.0000	0.0100 \pm 0.0000	0.0100 \pm 0.0000	0.0050 \pm 0.0000	0.0000 \pm 0.0000	0.0000 \pm 0.0000
L3	0.0000 \pm 0.0000					
L3 + KG	0.0000 \pm 0.0000					
L3-FT(Med)	0.0031 \pm 0.0027	0.0067 \pm 0.0058	0.0043 \pm 0.0037	0.0021 \pm 0.0019	0.0000 \pm 0.0000	0.0000 \pm 0.0000
L3-FT(Med) + KG	0.0000 \pm 0.0000					
L3-FT(QA)	0.4239 \pm 0.0343	0.3967 \pm 0.0513	0.4096 \pm 0.0435	0.2582 \pm 0.0341	0.7333 \pm 0.1155	0.7000 \pm 0.1732
L3-FT(QA) + KG	0.4552 \pm 0.0568	0.4467 \pm 0.0635	0.4509 \pm 0.0600	0.2924 \pm 0.0512	0.8000 \pm 0.0000	0.7667 \pm 0.0577
G-Retriever	0.3598 \pm 0.0387	0.3000 \pm 0.0520	0.3270 \pm 0.0467	0.1961 \pm 0.0340	0.8000 \pm 0.0000	0.7667 \pm 0.1155
GALAX	0.4900\pm0.0100	0.4900\pm0.0100	0.4900\pm0.0100	0.3245\pm0.0088	1.0000\pm0.0000	0.9000\pm0.0000

Table 28: Model performances on LAML

Model	Precision \uparrow	Recall \uparrow	F1 \uparrow	Jaccard \uparrow	Hit@5 \uparrow	Hit@10 \uparrow
M2T	0.0164	0.0100	0.0124	0.0062	0.0000	0.0000
GAT	0.0000 \pm 0.0000					
L3	0.0000 \pm 0.0000					
L3 + KG	0.1576 \pm 0.1412	0.0200 \pm 0.0173	0.0354 \pm 0.0307	0.0182 \pm 0.0158	0.1333 \pm 0.2309	0.2000 \pm 0.1732
L3-FT(Med)	0.1136 \pm 0.0630	0.0400 \pm 0.0173	0.0495 \pm 0.0088	0.0254 \pm 0.0004	0.2000 \pm 0.3464	0.1333 \pm 0.1528
L3-FT(Med) + KG	0.1085 \pm 0.0867	0.0267 \pm 0.0058	0.0377 \pm 0.0221	0.0193 \pm 0.0114	0.2000 \pm 0.3464	0.2000 \pm 0.1732
L3-FT(QA)	0.4758 \pm 0.0251	0.3733 \pm 0.0115	0.4180 \pm 0.0082	0.2642 \pm 0.0066	0.8667 \pm 0.2309	0.9000\pm0.1000
L3-FT(QA) + KG	0.4988\pm0.0700	0.4500\pm0.0600	0.4721\pm0.0572	0.3102\pm0.0481	0.8667 \pm 0.2309	0.8333 \pm 0.1155
G-Retriever	0.3719 \pm 0.0373	0.2400 \pm 0.0000	0.2912 \pm 0.0119	0.1705 \pm 0.0081	1.0000\pm0.0000	0.9000\pm0.0000
GALAX	0.4730 \pm 0.0901	0.4333 \pm 0.0306	0.4510 \pm 0.0554	0.2923 \pm 0.0467	0.9333 \pm 0.1155	0.8667 \pm 0.2309

Table 29: Model performances on DLBC

Model	Precision \uparrow	Recall \uparrow	F1 \uparrow	Jaccard \uparrow	Hit@5 \uparrow	Hit@10 \uparrow
M2T	0.0000	0.0000	0.0000	0.0000	0.0000	0.0000
GAT	0.0000 \pm 0.0000					
L3	0.0000 \pm 0.0000					
L3 + KG	0.0000 \pm 0.0000					
L3-FT(Med)	0.0220 \pm 0.0249	0.0367 \pm 0.0404	0.0275 \pm 0.0308	0.0141 \pm 0.0159	0.0000 \pm 0.0000	0.0000 \pm 0.0000
L3-FT(Med) + KG	0.0375 \pm 0.0385	0.0067 \pm 0.0058	0.0111 \pm 0.0097	0.0056 \pm 0.0049	0.0667 \pm 0.1155	0.0333 \pm 0.0577
L3-FT(QA)	0.3985 \pm 0.0669	0.3900 \pm 0.0721	0.3942 \pm 0.0695	0.2470 \pm 0.0530	0.9333 \pm 0.1155	0.8333\pm0.0577
L3-FT(QA) + KG	0.4200 \pm 0.0230	0.4100 \pm 0.0173	0.4149 \pm 0.0200	0.2619 \pm 0.0158	0.8667 \pm 0.1155	0.7000 \pm 0.1000
G-Retriever	0.3196 \pm 0.0307	0.2767 \pm 0.0058	0.2963 \pm 0.0168	0.1740 \pm 0.0115	1.0000\pm0.0000	0.8000 \pm 0.0000
GALAX	0.4400\pm0.0000	0.4400\pm0.0000	0.4400\pm0.0000	0.2821\pm0.0000	0.8667 \pm 0.1155	0.6333 \pm 0.2309

Table 30: Model performances on MM

Model	Precision \uparrow	Recall \uparrow	F1 \uparrow	Jaccard \uparrow	Hit@5 \uparrow	Hit@10 \uparrow
M2T	0.0000	0.0000	0.0000	0.0000	0.0000	0.0000
GAT	0.0000 \pm 0.0000					
L3	0.0000 \pm 0.0000					
L3 + KG	0.0000 \pm 0.0000					
L3-FT(Med)	0.0275 \pm 0.0296	0.0167 \pm 0.0208	0.0156 \pm 0.0149	0.0079 \pm 0.0075	0.0667 \pm 0.1155	0.0333 \pm 0.0577
L3-FT(Med) + KG	0.1091 \pm 0.0630	0.0200 \pm 0.0000	0.0329 \pm 0.0027	0.0167 \pm 0.0014	0.1333 \pm 0.1155	0.1333 \pm 0.1155
L3-FT(QA)	0.4001 \pm 0.0022	0.3800 \pm 0.0265	0.3894 \pm 0.0134	0.2418 \pm 0.0103	0.9333 \pm 0.1155	0.9000 \pm 0.0000
L3-FT(QA) + KG	0.4753 \pm 0.0613	0.4367 \pm 0.0306	0.4549 \pm 0.0447	0.2952 \pm 0.0377	0.8000 \pm 0.0000	0.7333 \pm 0.0577
G-Retriever	0.4514 \pm 0.0890	0.3667 \pm 0.0808	0.4046 \pm 0.0850	0.2561 \pm 0.0690	0.9333 \pm 0.1155	0.9000 \pm 0.0000
GALAX	0.5858\pm0.0564	0.5700\pm0.0819	0.5775\pm0.0695	0.4082\pm0.0680	1.0000\pm0.0000	0.9333\pm0.0577

Table 31: Model performances on KIRC

Model	Precision \uparrow	Recall \uparrow	F1 \uparrow	Jaccard \uparrow	Hit@5 \uparrow	Hit@10 \uparrow
M2T	0.0000	0.0000	0.0000	0.0000	0.0000	0.0000
GAT	0.0000 \pm 0.0000					
L3	0.0000 \pm 0.0000					
L3 + KG	0.0000 \pm 0.0000					
L3-FT(Med)	0.0000 \pm 0.0000					
L3-FT(Med) + KG	0.0000 \pm 0.0000					
L3-FT(QA)	0.5458 \pm 0.0450	0.5333 \pm 0.0513	0.5394 \pm 0.0478	0.3703 \pm 0.0452	0.8667 \pm 0.2309	0.8667 \pm 0.1155
L3-FT(QA) + KG	0.4897 \pm 0.0182	0.4800 \pm 0.0265	0.4847 \pm 0.0219	0.3201 \pm 0.0192	0.8667 \pm 0.1155	0.9000\pm0.0000
G-Retriever	0.4160 \pm 0.0315	0.3733 \pm 0.0058	0.3933 \pm 0.0171	0.2449 \pm 0.0133	0.6000 \pm 0.0000	0.8000 \pm 0.0000
GALAX	0.5797\pm0.0251	0.5700\pm0.0265	0.5748\pm0.0254	0.4036\pm0.0247	0.9333\pm0.1155	0.9000\pm0.1732

Table 32: Model performances on THCA

Model	Precision \uparrow	Recall \uparrow	F1 \uparrow	Jaccard \uparrow	Hit@5 \uparrow	Hit@10 \uparrow
M2T	0.0000	0.0000	0.0000	0.0000	0.0000	0.0000
GAT	0.0000 \pm 0.0000					
L3	0.0000 \pm 0.0000					
L3 + KG	0.1500 \pm 0.1500	0.0200 \pm 0.0173	0.0348 \pm 0.0303	0.0179 \pm 0.0155	0.1333 \pm 0.2309	0.1000 \pm 0.1732
L3-FT(Med)	0.0439 \pm 0.0532	0.0167 \pm 0.0058	0.0200 \pm 0.0119	0.0101 \pm 0.0061	0.0667 \pm 0.1155	0.0333 \pm 0.0577
L3-FT(Med) + KG	0.0156 \pm 0.0145	0.0300 \pm 0.0265	0.0205 \pm 0.0187	0.0104 \pm 0.0095	0.0000 \pm 0.0000	0.0333 \pm 0.0577
L3-FT(QA)	0.5495 \pm 0.0165	0.5367 \pm 0.0153	0.5430 \pm 0.0158	0.3728 \pm 0.0148	0.8667 \pm 0.1155	0.8333 \pm 0.0577
L3-FT(QA) + KG	0.5818 \pm 0.0490	0.5333 \pm 0.0416	0.5556 \pm 0.0365	0.3853 \pm 0.0353	0.9333 \pm 0.1155	0.9000 \pm 0.1000
G-Retriever	0.6237\pm0.0849	0.3833 \pm 0.0231	0.4718 \pm 0.0097	0.3088 \pm 0.0083	0.5333 \pm 0.1155	0.7333 \pm 0.1155
GALAX	0.6076 \pm 0.0331	0.6033\pm0.0289	0.6054\pm0.0308	0.4346\pm0.0313	1.0000\pm0.0000	1.0000\pm0.0000

Table 33: Model performances on BLCA

Model	Precision \uparrow	Recall \uparrow	F1 \uparrow	Jaccard \uparrow	Hit@5 \uparrow	Hit@10 \uparrow
M2T	0.0000	0.0000	0.0000	0.0000	0.0000	0.0000
GAT	0.0000 \pm 0.0000					
L3	0.0000 \pm 0.0000					
L3 + KG	0.0000 \pm 0.0000					
L3-FT(Med)	0.0127 \pm 0.0111	0.0267 \pm 0.0231	0.0172 \pm 0.0149	0.0087 \pm 0.0076	0.0000 \pm 0.0000	0.0000 \pm 0.0000
L3-FT(Med) + KG	0.0222 \pm 0.0385	0.0033 \pm 0.0058	0.0058 \pm 0.0100	0.0029 \pm 0.0051	0.0000 \pm 0.0000	0.0333 \pm 0.0577
L3-FT(QA)	0.5538 \pm 0.0498	0.5000 \pm 0.0200	0.5250 \pm 0.0301	0.3563 \pm 0.0279	0.7333 \pm 0.1155	0.8000 \pm 0.0000
L3-FT(QA) + KG	0.5617\pm0.0584	0.5367\pm0.0231	0.5484\pm0.0376	0.3784\pm0.0356	0.8667 \pm 0.2309	0.8667 \pm 0.0577
G-Retriever	0.5025 \pm 0.0481	0.4733 \pm 0.0058	0.4870 \pm 0.0253	0.3221 \pm 0.0223	0.6000 \pm 0.0000	0.6333 \pm 0.0577
GALAX	0.5247 \pm 0.0081	0.5033 \pm 0.0289	0.5133 \pm 0.0115	0.3453 \pm 0.0104	1.0000\pm0.0000	0.9000\pm0.1000

Table 34: Model performances on UCEC

Model	Precision \uparrow	Recall \uparrow	F1 \uparrow	Jaccard \uparrow	Hit@5 \uparrow	Hit@10 \uparrow
M2T	0.0000	0.0000	0.0000	0.0000	0.0000	0.0000
GAT	0.0000 \pm 0.0000					
L3	0.0000 \pm 0.0000					
L3 + KG	0.0000 \pm 0.0000					
L3-FT(Med)	0.0000 \pm 0.0000					
L3-FT(Med) + KG	0.0000 \pm 0.0000					
L3-FT(QA)	0.5293\pm0.0394	0.5133 \pm 0.0379	0.5211 \pm 0.0379	0.3530 \pm 0.0344	0.7333 \pm 0.1155	0.7000 \pm 0.1000
L3-FT(QA) + KG	0.4672 \pm 0.0472	0.4533 \pm 0.0231	0.4600 \pm 0.0346	0.2991 \pm 0.0296	0.8000 \pm 0.2000	0.8000 \pm 0.1000
G-Retriever	0.4517 \pm 0.0318	0.4000 \pm 0.0173	0.4242 \pm 0.0237	0.2694 \pm 0.0193	1.0000\pm0.0000	0.9000\pm0.0000
GALAX	0.5280 \pm 0.0555	0.5233\pm0.0635	0.5256\pm0.0596	0.3579\pm0.0536	0.8000 \pm 0.0000	0.9000\pm0.0000

Table 35: Model performances on PRAD

Model	Precision \uparrow	Recall \uparrow	F1 \uparrow	Jaccard \uparrow	Hit@5 \uparrow	Hit@10 \uparrow
M2T	0.0000	0.0000	0.0000	0.0000	0.0000	0.0000
GAT	0.0000 \pm 0.0000					
L3	0.0111 \pm 0.0192	0.0033 \pm 0.0058	0.0051 \pm 0.0089	0.0026 \pm 0.0045	0.0000 \pm 0.0000	0.0000 \pm 0.0000
L3 + KG	0.0000 \pm 0.0000					
L3-FT(Med)	0.0145 \pm 0.0251	0.0033 \pm 0.0058	0.0054 \pm 0.0094	0.0027 \pm 0.0047	0.0000 \pm 0.0000	0.0000 \pm 0.0000
L3-FT(Med) + KG	0.0176 \pm 0.0261	0.0067 \pm 0.0058	0.0078 \pm 0.0083	0.0039 \pm 0.0042	0.0000 \pm 0.0000	0.0333 \pm 0.0577
L3-FT(QA)	0.6021 \pm 0.0558	0.5600 \pm 0.0400	0.5796 \pm 0.0401	0.4088 \pm 0.0392	1.0000\pm0.0000	0.9333 \pm 0.1155
L3-FT(QA) + KG	0.6032\pm0.0191	0.5867\pm0.0115	0.5947\pm0.0102	0.4232\pm0.0103	0.9333 \pm 0.1155	0.9000 \pm 0.1000
G-Retriever	0.4749 \pm 0.0041	0.4433 \pm 0.0231	0.4584 \pm 0.0141	0.2974 \pm 0.0120	1.0000\pm0.0000	1.0000\pm0.0000
GALAX	0.5152 \pm 0.1398	0.4733 \pm 0.0751	0.4923 \pm 0.1036	0.3308 \pm 0.0934	0.9333 \pm 0.1155	0.9667 \pm 0.0577